The Vibration of Perforated Hemispherical Shells

M.A. Sprague

August 1997

UWFDM-1049

FUSION TECHNOLOGY INSTITUTE

UNIVERSITY OF WISCONSIN

MADISON WISCONSIN

The Vibration of Perforated Hemispherical Shells

M.A. Sprague

Fusion Technology Institute
University of Wisconsin
1500 Engineering Drive
Madison, WI 53706

http://fti.neep.wisc.edu

August 1997

UWFDM-1049

The Vibration of Perforated Hemispherical Shells

by

Michael Alan Sprague

A thesis submitted in partial fulfillment of the requirements for the degree of

Bachelor of Science

(Mechanical Engineering)

at the

University of Wisconsin–Madison

1997

Abstract

The Vibration of Perforated Hemispherical Shells

Michael Alan Sprague
Under the Supervision of Professor Roxann Louise Engelstad

Hemispherical shells used for inertial confinement fusion reactor target chamber components may require various perforation patterns for beam lines, diagnostic equipment, and target insertion. For design and analysis purposes, the natural frequencies of these shells must be known. This research investigated the axisymmetric vibrations of clamped perforated hemispherical shells using the finite element method. Shells with an apex hole and shells with circumferential holes in addition to the apex hole were studied. The nondimensional frequencies were identified for the first three axisymmetric modes for a shell with a wide range of apex hole sizes and shell thickness. It was shown that a clamped hemispherical shell's response to a uniform radial impulse load was dominated by modes with frequencies considerably higher than the fundamental frequency. This behavior was seen in all clamped hemispherical shells studied. With damping neglected, the dominant impulse response frequencies were presented for each shell tested. The shell with circumferential holes in addition to the apex hole responded to the impulse load in a manner approaching an axisymmetric condition. The frequencies of these quasi-axisymmetric modes were identified up to the thirteenth mode for the shell tested. This investigation has demonstrated that a uniform hemispherical shell can be used to accurately approximate the dynamic behavior of a hemispherical shell with relatively small perforations.

Approved:

Professor Roxann Louise Engelstad
University of Wisconsin–Madison
Mechanical Engineering

Acknowledgment

I would like to thank my parents and Hollie Brouwer for their patience and support throughout my undergraduate career. I would like to express my gratitude to Prof. Edward Lovell for his availability to answer questions and his extensive knowledge of shell vibration issues. I am deeply indebted to Prof. Roxann Engelstad for allowing me the opportunity to perform this research, and for her support throughout this investigation. My time spent under her guidance has been an invaluable learning experience.

Table of Contents

List of Figures

List of Tables

List of Symbols

a	apex hole radius
b	circumferential hole radius
c	shell base half span
E	elastic modulus of material
f	frequency, Hz
h	shell thickness
h_{AVG}	average shell thickness
H	shell height
i	circumferential wave number
m	meridonal wave number
P	pressure
r	radial coordinate
R	shell midsurface radius
t	time
u	circumferential displacement
v	meridonal displacement
w	radial displacement
$w_{,\phi}$	rotation of normal to shell surface
β_ϕ	rotation of normal to shell surface
β_θ	rotation of normal to shell surface
θ	circumferential coordinate
υ	Poisson's ratio
ρ	shell mass density
ϕ	meridonal coordinate
ϕ_0	shell meridonal half-angle
ϕ_a	meridonal half-angle of apex hole
ϕ_b	meridonal angle from apex to axis of circumferential hole
ω	circular frequency, rad/s
Ω	nondimensional frequency, $\sqrt{\frac{\rho\omega^2 R^2\left(1-\upsilon^2\right)}{E}}$

Ω' classic nondimensional frequency, $\sqrt{\frac{\rho\omega^2 R^2}{E}}$

Ω_T nondimensional frequency of the first shear mode (thickness mode) of an infinite plate

Chapter 1

Introduction

1.1 Introduction

The primary goal of this research is to aid in the design of hemispherical endcaps for use in inertial confinement fusion reactor target chambers. Any shell structure used in a target chamber may require various holes, or perforation patterns, for diagnostic equipment, target insertion, and beam lines. To properly design a target chamber, the natural frequencies of the structure must be known to prevent catastrophic failures due to resonant conditions. Currently, methods exist for accurately calculating the natural frequencies of uniform hemispherical shells. This research is concerned with finding the natural frequencies of perforated hemispherical shells, for which no known analytical solution exists. In addition, no work regarding the dynamic behavior of deep perforated spherical shell segments has been found by the author. Because of the impossibility of generating an analytical solution, finite element (FE) models were used in this analysis to identify numerical values for the natural frequencies of the axisymmetric vibration of several perforated hemispherical shells.

1.2 Inertial Confinement Fusion (ICF)

Fusion energy is released from a reaction between two light nuclei when they combine to form a single nucleus. It is the energy of the sun. If implemented, it could be a virtually inexhaustible energy source for the earth. Fusion could remove much of the need to burn fossil fuels that are unkind to the earth's atmosphere. The radiological hazards associated with fusion power are hundreds of times less than those of fission, and the process releases no greenhouse gases [1.1].

One proposed method to produce fusion energy is Inertial Confinement Fusion (ICF). It is produced by focusing beams of either accelerated ions or laser light on targets filled with hydrogen. The beams force the target to implode, thereby squeezing the nuclei together so a fusion reaction occurs [1.1].

An ICF power plant would consist of drivers, a target factory, a target chamber, and steam turbines. Targets, small capsules containing fuel such as deuterium-tritium, would be manufactured and injected in the target chamber. Beams of either accelerated ions or laser light from the driver would be focused on the target to induce the fusion reaction. Heat from the reaction would be captured in the target chamber and converted to usable energy through the steam turbine [1.1].

1.3 National Ignition Facility (NIF)

The first step towards an ICF power plant would be the construction of the proposed National Ignition Facility (NIF) at the Lawrence Livermore National Laboratory (see Figs. 1.1 and 1.2). If constructed, it would use lasers to induce fusion reactions. Its primary purpose would be defense, but would also be used to study issues associated with implementing fusion as a viable energy source. These include target chamber dynamics, target physics, ICF fusion power technologies, and target systems [1.2].

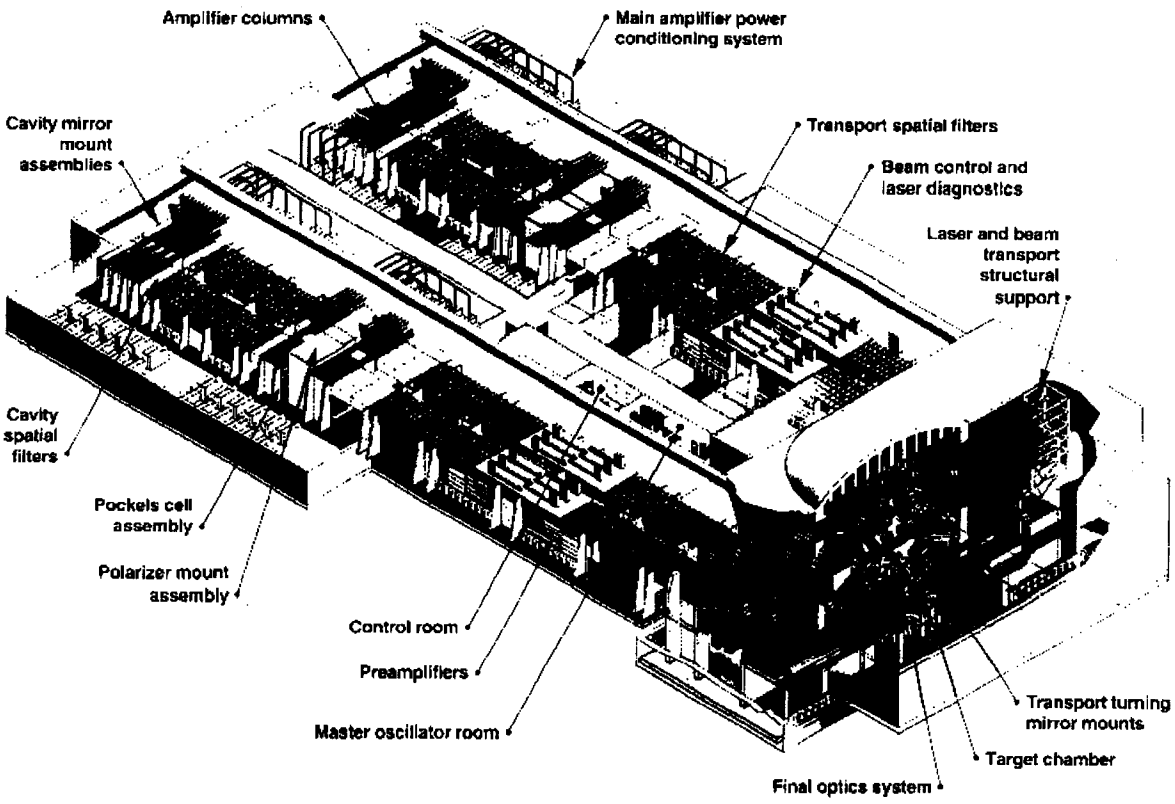

Fig. 1.1. The National Ignition Facility [1.2].

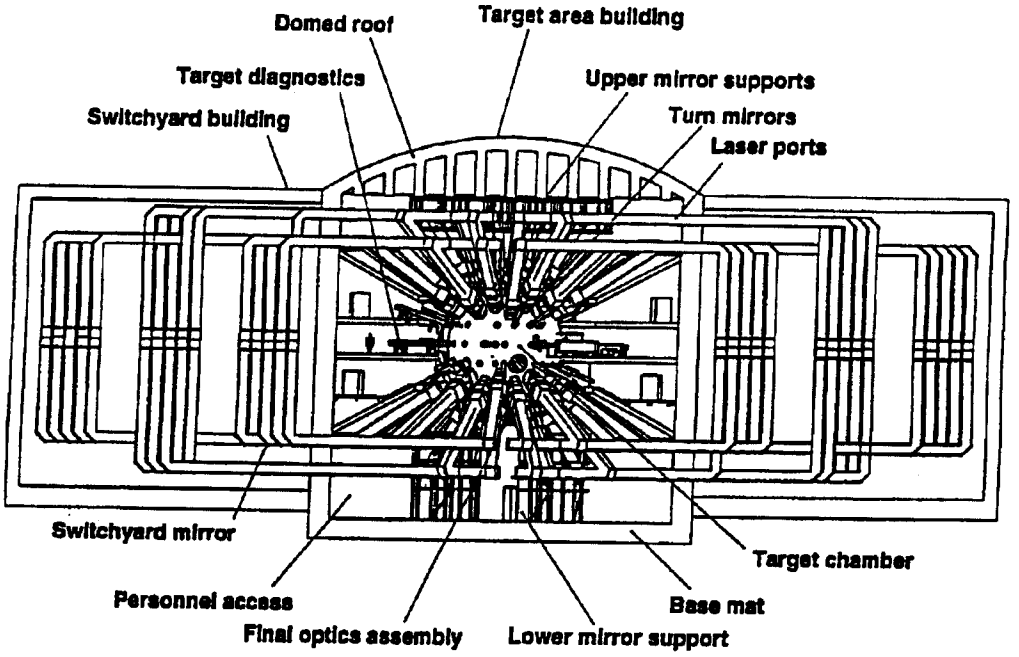

Fig. 1.2. The NIF target area [1.2].

This research is concerned with target chamber dynamics. Several designs have been proposed for the target chamber [1.3, 1.4], as shown in Figs. 1.3 and 1.4. All designs require perforation patterns for diagnostic equipment, laser ports, target insertion, and target maintenance.

1.4 Thesis Overview

Chapter 2 will discuss previous work on the vibrations of deep spherical shells. It will be shown that no work has been done for deep, perforated, spherical shells. Chapter 3 will present the coordinate system used throughout this analysis, and discuss the nondimensional frequency parameters used for spherical shells. The geometry of the shells to be tested will then be introduced. The FE method used for studying the vibration of spherical shells will be verified in Chapter 4. Chapter 5 will present numerical results for the axisymmetric natural frequencies of a clamped hemispherical shell with an apex hole. The response of the shell to a uniform radial impulse load will be investigated in Chapter 6. Chapter 7 is concerned with the response of a clamped hemispherical shell with circumferential holes in addition to the apex hole to an impulse load. Chapter 8 will summarize the conclusions made in this research.

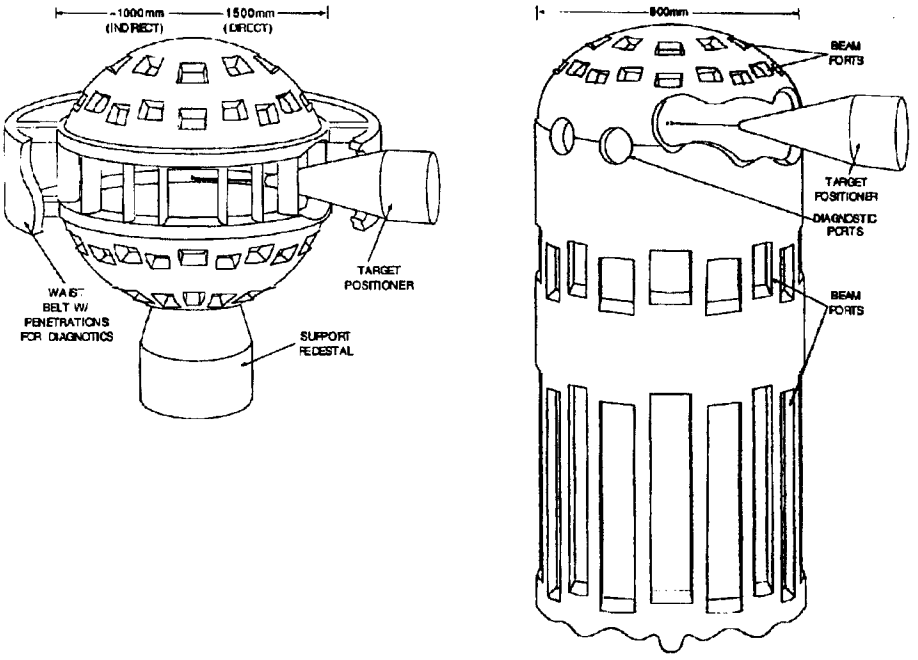

Fig. 1.3. Proposed target mini-chambers for the NIF [1.3].

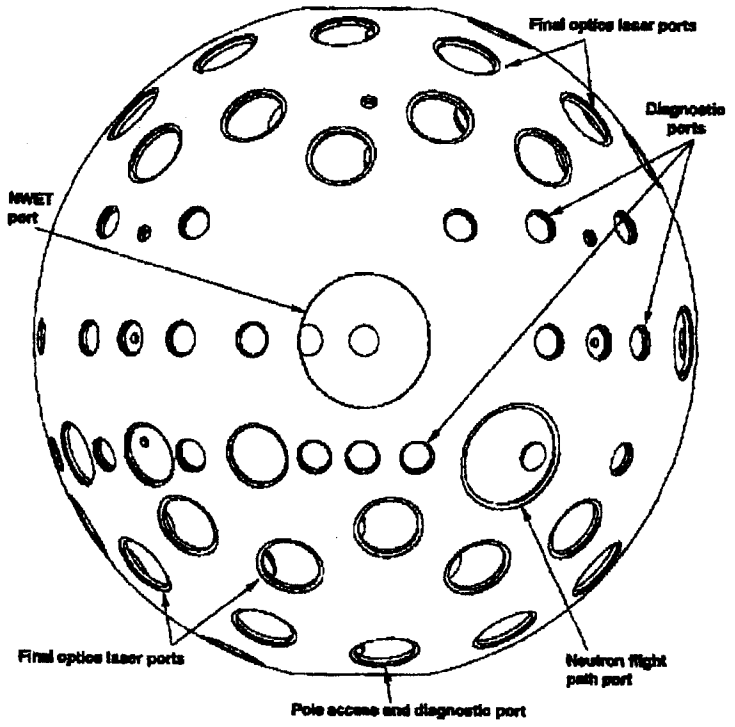

Fig. 1.4. Proposed target chamber for the NIF [1.4].

1.5 References

[1.1] "Alternative Paths to Fusion," UCRL-TB-124383, Lawrence Livermore National Laboratory, 1996.

[1.2] Logan, B. G., Tobin, M. T., and Meier, W. R., "The Role of the National Ignition Facility in the Development of Inertial Fusion Energy," Lawrence Livermore National Laboratory, W. J. Schafer Associates, Inc., UCRL-ID-119383, 1995.

[1.3] Peterson, P. F., and Scott, J. M., "The Mini-Chamber, an Advanced Protection Concept for NIF," *Proceedings from the 12th Annual Conference of the American Nuclear Society*, 1996.

[1.4] Streckert, H. H., et al., "Conceptual Design of Low Activation Target Chamber and Components for the National Ignition Facility," *Proceedings from the 12th Annual Conference of the American Nuclear Society*, 1996.

Chapter 2

Literature Survey

2.1 Literature Survey

The study of the vibration of shells of revolution began in 1881 with Lord Rayleigh's [2.1] inextensional analysis. His work was aimed at the calculation of the natural frequencies of bells. The first extensional analysis was performed by Lamb [2.2] in 1882 in a study on the vibrations of closed spherical shells. As shown by De Souza and Croll [2.3], Rayleigh and Lamb were both correct in their extensional or inextensional approximations. The low-frequency modes for open spherical shells are composed almost entirely of bending energy, whereas the low-frequency modes of closed spherical shells are "dominated by the membrane contribution to stiffness" [2.3].

"Classical thin shell theory" was developed by Love [2.4] using what is now known as Love's first approximation. This was the first work to combine both bending and membrane deformations in the analysis. Other early studies of spherical shell vibrations were carried out by Zwingli [2.5] and Federhofer [2.6].

The next phase in thin shell theory was initiated by the needs of the aerospace and nuclear industries where the simplifying approximations of Rayleigh and Lamb were no longer adequate [2.3]. In 1956, Naghdi [2.7] developed the equations of motion for thin, elastic, isotropic shells of uniform thickness, which included the effects of transverse normal stress, transverse shear deformation, as well as rotary inertia. A complete solution for the free vibration of deep spherical shells had to await the 1962 work of Naghdi and Kalnins [2.8]. This work reduced the basic equations of Love's first approximation to a system of two coupled differential equations. Numerical solutions for the torsionless axisymmetric vibration of a hemispherical shell with a free edge were presented. Their results implied that the vibrations of the hemispherical shell studied were primarily extensional. Because of this, and the computational difficulties associated with calculating asymmetric vibrations using general shell bending theory, the asymmetric modes were studied using the more simplistic extensional theory.

Numerical values were presented and compared to those found using Rayleigh's [2.1] inextensional approximation.

The study of deep open spherical shells was taken further with the work of Kalnins [2.9] in 1964 with an analysis based on the "linear classical bending theory of shells" from the works of Naghdi and Kalnins [2.8] and Federhofer [2.6]. This investigation presented numerical results for the axisymmetric vibration of a deep spherical shell with various edge conditions, including the clamped case. The shell studied had a shell half-angle, ϕ_0, of 60°, and a thickness-to-radius ratio, h/R, of 0.05. Kalnins showed that extensional theory is capable of accurately predicting the membrane modes, but may produce considerable error in predicting bending modes, especially if bending is neglected in the formulation of the governing equations. Kalnins showed that the membrane modes were essentially the degenerate case of the bending modes, and these were independent of thickness. It was also shown that neglecting tangential inertia terms is not justified for deep spherical shells, and that open spherical shell modes of free vibration can be separated into two basic groups, i.e., bending and membrane modes.

Prasad [2.10] presented the equations of motion for deep open spherical shells reduced to a system of two uncoupled equations and one partly coupled equation. As an example, he solved the equations of motion for a hemispherical shell with a clamped edge. The results were presented in terms of associated Legendre functions. Prasad claimed that his solution included the effects of transverse shear deformation as well as rotary inertia. This claim was attacked by Jahanshahi [2.11], who specialized the equations of Naghdi's [2.7] work for the case of deep spherical shells. Naghdi's equations included the effects of transverse shear deformation, rotary inertia, and normal stress. Jahanshahi showed that Prasad's final system of equations disagree with those derived from the specialized (or reduced) set of Naghdi's equations, and questioned why certain terms were neglected in Prasad's analysis.

Wilkinson and Kalnins [2.12] derived solutions for the dynamic deformation of spherical shells which included the effects of rotary inertia and transverse shear deformation. This analysis retained the appropriate inertia terms neglected by Prasad

[2.10]. It was shown that the effects of rotary inertia and transverse shear deformation are of negligible importance in the low-frequency range, but affect the higher frequency solutions. It was also shown that drastic changes are expected to occur in the solution where the nondimensional spherical shell frequency, Ω, equals the frequency of the first shear mode (or thickness mode) of an infinite plate, Ω_T. Kalnins and Kraus [2.13] extended this analysis to the free vibration of hemispherical and closed spherical shells. It was shown that as Ω approaches Ω_T, the improved theory reveals modes not predicted by classical theory. It was also shown that if transverse shear deformation is neglected in the analysis, but rotary inertia is maintained, the results are almost the same as those derived using classical theory.

Ross [2.14] performed an approximate analysis of the axisymmetric vibrations of deep spherical shells based on the work of Kalnins [2.9]. Whereas Kalnins used a numerical analysis to solve the differential equations, Ross utilized the asymptotic formulas for Legendre functions with large arguments to generate an approximate solution in closed form. The axisymmetric natural frequencies generated using this method are the same as those generated using membrane theory. This approximation was shown to be in good agreement with the results of Kalnins except where the classic nondimensional frequency, Ω' (which neglects effects of Poisson's ratio), approaches unity. It was also shown that no bending frequencies occur where $\Omega' < 1$.

One of the first finite element analyses of the axisymmetric vibrations of deep spherical shells was performed by Navaratna [2.15] in 1966. A finite element model of a deep spherical shell ($\phi_0 = 60°$, $h/R = 0.05$) with 100 degrees of freedom was created and tested with various boundary conditions. The results were compared to those of Ross [2.14] and Kalnins [2.9], which neglected torsional vibrations. The values compared very well with those of Kalnins, but introduced torsional modes of vibration that were missed by both Kalnins and Ross.

Hwang [2.16] performed the first experimental work on the vibrations of deep spherical shells. The experiments investigated the axisymmetric and asymmetric vibrations of an aluminum hemispherical shell with a free edge and constant thickness. The results were compared with those found using several analytical methods. Using

the general bending shell theory of Naghdi and Kalnins [2.8], Hwang showed that the axisymmetric vibrations corresponded well with theory. However, he claimed that general shell theory failed to predict the asymmetric modes seen in the experiment, and showed that the inextensional approximation of Rayleigh [2.1] yields acceptable results. Hwang attributed the failure of general shell theory to predict asymmetric modes to either computational error, or inherent errors in the theory. Kalnins [2.17], in a later letter, states that its failure must be attributed to computational errors. Kalnins claimed that the inextensional theory is a special case of the general bending theory of shells, and it cannot be true that the general shell theory is incapable of predicting the inextensional modes if they are predicted by the inextensional theory, and if they actually occur.

In 1965, Zarghamee and Robinson [2.18] studied the asymmetric vibrations of spherical shells using an approximate asymptotic analysis. They presented a later work [2.19] in which the asymmetric frequencies were found using the Holzer method, which was originally developed for the determination of the torsional frequencies of a vibrating shaft. Zharghamee and Robinson generalized the method to be used in the analysis of the free vibration of spherical shells. It was shown that the Holzer method gave results that corresponded well with their earlier approximation, but the method is not applicable to extremely thin shells.

In Russia, approximate analyses of the asymmetric vibrations of deep spherical shells were presented in 1969 by Shmakov [2.20]. Based on the equations of motion of Shmakov, solutions for the asymmetric vibration of deep spherical shells were also developed by Valikov and Gots [2.21] using numerical methods. The solutions to the differential equations of motion were presented in the "form of rapidly converging series of Legendre functions and their derivatives." Numerical values for the clamped edge case were presented for two h/R values. Later work from Valikov and Gots [2.22] was presented in 1972. In 1973, Martynenko and Shpakova [2.23] presented an exact analysis of the asymmetric vibrations of spherical shells. The results of this work contradicted those found by Valikov and Gots [2.22]. Martynenko and Shpakova stated that the analysis of Valikov and Gots was incorrect since it neglected the effects of normal rotation in the governing equations of motion.

The first experiments on the axisymmetric vibrations of a clamped edge hemispherical shell were performed by Eikrem and Doige [2.24]. The shell had a radius of 6 in., and a thickness that varied from 0.023 in. at the edge, to 0.045 in. at the apex. Their results were compared to analytical values derived from the differential equations of motion of Naghdi and Kalnins [2.8], which neglected transverse shear deformation and rotary inertia. An average shell thickness, h_{AVG}, of 0.031 in. was used in the analytical analysis. Analytical and experimental values were carried out to the 23rd flexural axisymmetric mode. The experimental modes agreed well with the analytical results, but failed to identify the modes in the region where $\Omega' \approx 1$. The experiment also failed to show the first and second extensional modes which occur at $\Omega' = 1.663$ and $\Omega' = 2.837$, respectively, for the shell tested.

Using a finite difference modeling of "classical" thin shell formulation, De Souza and Croll [2.3] studied open spherical shells ranging from a shallow cap to a hemispherical dome. The coordinate frame chosen for the finite difference analysis caused singularities to occur at the apex. To overcome this singularity, De Souza and Croll placed a hole with a small half-angle, ϕ_a, at the apex of all shells studied. It was shown that an apex hole with $\phi_a / \phi_0 << 1$, for practical purposes, has negligible effects. The analysis showed how membrane and bending stiffness contribute to a shell's resistance to both axisymmetric and asymmetric vibrations. It was shown that decreasing the thickness-to-radius ratios increases the membrane energy associated with the low-frequency vibration modes. For deep spherical shells, the vibrations associated with the lowest circumferential wave numbers, i, are mostly composed of meridonal membrane energy. Circumferential membrane action and membrane shear action also contribute significant energy to the total energy of the system for low values of i. Higher values of i are dominated by circumferential bending energy. It was also shown that decreasing the depth of an open shell increases the contributions of bending energy. Numerical results included the axisymmetric and asymmetric vibrations of a clamped-edge hemispherical shell with $h/R = 0.005$.

Using a finite element analysis based on the shell theory of Naghdi [2.7], Singh and Mirza [2.25] presented numerical results for the asymmetric modes of deep spherical

shells with ϕ_0 ranging from 30° to 90°. Boundary conditions included the clamped edge and hinged edge cases. The analysis included the effects of shear deformation and rotary inertia. The spherical shells analyzed by Singh and Mirza, like those studied by De Souza and Croll [2.3], had a small hole at the apex to remove the singularity effects that occur in the equations of motion at the apex for asymmetric vibrations. The half-angle of the apex hole was taken to be 0.125% of the shell half-angle, ϕ_0.

2.2 References

[2.1] Rayleigh, "On the Infinitesimal Bending of Surfaces of Revolution," *Proceedings of the London Mathematical Society*, Vol. 13, 1881, pp. 4-16.

[2.2] Lamb, H., "On the Vibrations of a Spherical Shell," *Proceedings of the London Mathematical Society,* Vol. 14, 1882, pp. 50-56.

[2.3] De Souza, V. C. M., and Croll, J. G. A., "An Energy Analysis of the Free Vibrations of Isotropic Spherical Shells," *The Journal of Sound and Vibration*, Vol. 73, No. 3, 1980, pp. 379-404.

[2.4] Love, A. E. H., "The Small Free Vibrations and Deformation of a Thin Elastic Shell," *Philosophical Transactions of the Royal Society*, London, England, Series A, Vol. 179, 1888, pp. 491-546.

[2.5] Zwingli, H., "Elastische Schwingungen von Kugelschalen," Dissertation, Tech. Hochschule in Zurich, 1930.

[2.6] Federhofer, K., "Sur Berechnung der Eigenschwingungen der Kugelshale," *Mathematisch-naturwissenschaftliche Klasse,* Vol. 146 2A, 1937, pp. 57-69 and 505-514.

[2.7] Naghdi, P. M., "On the Theory of Thin Elastic Shells," *Quarterly of Applied Mathematics*, Vol. 14, 1957, pp. 369-380.

[2.8] Naghdi, P. M., and Kalnins, A., " On Vibrations of Elastic Spherical Shells," *Journal of Applied Mechanics,* Vol. 29, 1962, pp. 65-72.

[2.9] Kalnins, A., "Effect of Bending on Vibrations of Spherical Shells," *The Journal of the Acoustical Society of America*, Vol. 36, No. 1, 1964, pp. 74-81.

[2.10] Prasad, C., "On Vibrations of Spherical Shells," *The Journal of the Acoustical Society of America,* Vol. 36, No. 3, 1964, pp. 489-494.

[2.11] Jahanshahi, A., "Equations of Motion of Spherical Shells," *The Journal of the Acoustical Society of America,* Vol. 38, No. 5, 1965, pp. 883-885.

[2.12] Wilkinson, J. P., and Kalnins, A., "On Nonsymmetric Dynamic Problems of Elastic Spherical Shells," *Journal of Applied Mechanics*, Vol. 32, 1965, pp. 525-532.

[2.13] Kalnins, A., and Kraus, H., "Effect of Transverse Shear and Rotary Inertia on Vibrations of Spherical Shells," *Proceedings of the 5th U.S. National Congress of Applied Mechanics*, 1966, p. 134.

[2.14] Ross, E. W. Jr., "Natural Frequencies and Mode Shapes for Axisymmetric Vibration of Deep Spherical Shells," *Journal of Applied Mechanics*, Vol. 32, No. 1, 1965, pp. 553-561.

[2.15] Navaratna, D. R., "Natural Vibrations of Deep Spherical Shells," *AIAA Journal*, Vol. 4, No. 11, 1966, pp. 2056-2058.

[2.16] Hwang, C., "Some Experiments on the Vibration of a Hemispherical Shell," *Journal of Applied Mechanics*, Vol. 33, 1966, pp. 817-824.

[2.17] Kalnins, A., "Some Experiments on the Vibration of a Hemispherical Shell," *Journal of Applied Mechanics*, Vol. 34, 1967, pp. 792-794.

[2.18] Zarghamee, M. S., and Robinson, A. R., "Free and Forced Vibrations of Spherical Shells," University of Illinois, Structural Research Series 293, July 1965.

[2.19] Zarghamee, M. S., and Robinson, A. R., "A Numerical Method for Analysis of Free Vibration of Spherical Shells," *AIAA Journal*, Vol. 5, No. 5, 1967, pp. 1256-1261.

[2.20] Shmakov, V. P., "On Vibrations of Nonshallow Spherical Shells," *Izvestiia Akademii Nauk SSSR, Mekhanika Tverdogo Tela*, No. 3, 1969.

[2.21] Valikov, K. V., and Gots, A. N., "Calculation of the Natural Frequencies of Spherical Shells," *Prikladnaya Mekhanika*, Vol. 7, No. 6, 1971, pp. 49-55.

[2.22] Valikov, K. V., and Gots, A. N., "On the Calculation of Free Vibrations of Thin Spherical Shells," *Izvestiia Vuzov, Matematika*, No. 11, 1972.

[2.23] Martynenko, V. S., and Shpakova, S. G., "Asymmetric Vibrations of Spherical Shells," *Prikladnaya Mekhanika*, Vol. 9, No. 10, 1973, pp. 23-28.

[2.24] Eikrem, A. K. A., and Doige, A. G., "Natural Frequencies of a Hemispherical Shell," *Experimental Mechanics*, Vol. 12, No. 12, 1972, pp. 575-579.

[2.25] Singh, A. V., and Mirza, S., "Asymmetric Modes and Associated Eigenvalues for Spherical Shells," *The Journal of Pressure Vessel Technology*, Vol. 107, 1985, pp. 77-82.

Chapter 3

Problem Formulation

3.1 Introduction

This chapter will present the problem formulation for this research, which is focused solely on perforated hemispherical shells; the coordinate system used and the nondimensional frequency parameters associated with spherical shells will be presented. The geometry of the perforated shells studied in this research will then be introduced. All shells investigated in this study were hemispherical, a category of deep shells. Shells are considered deep if the ratio of the shell height, H, to the base span, $2c$, is at least 1/8. If $H/2c$ is less than 1/8, the shell may be considered shallow, and simplifying assumptions, such as small angles, may be made in solving the governing equations of motion. For reference, a shallow spherical shell geometry definition is shown in Fig. 3.1.

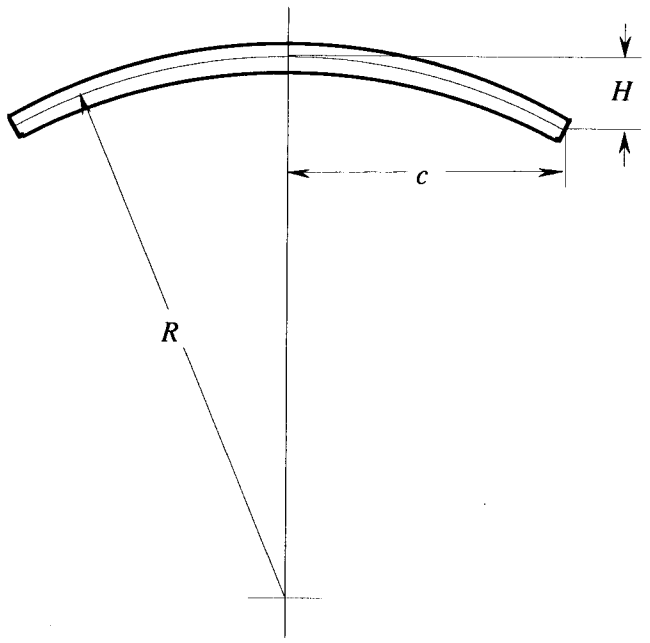

Fig. 3.1. Spherical shallow shell geometry.

3.2 Spherical Coordinate System

A spherical coordinate system, (r, θ, ϕ), was used throughout this analysis. It is shown in Fig. 3.2 with the (x, y, z) Cartesian coordinate system for reference. In addition, an element of the shell is shown with all associated displacements. The displacement normal to the shell is represented by w. Tangential circumferential displacement and tangential meridonal displacement are represented by v and u, respectively. Shell rotation symbols are not shown. The rotation of the shell normal about the shell normal vector is measured by $w,_{\phi}$. Rotation of the shell normal about tangential circumferential and meridonal vectors are β_{θ} and β_{ϕ}, respectively.

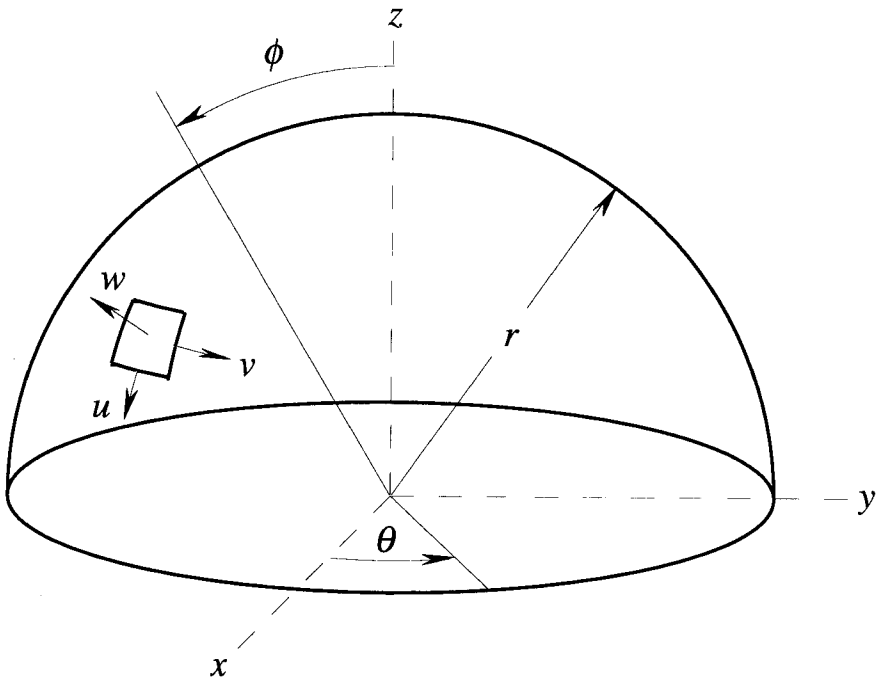

Fig. 3.2. Spherical coordinate system with shell displacement components.

3.3 Thin Shell Definition

All shells studied in this research are considered "thin," i.e., $h/R << 1$. In the study of thin shells, the outer surfaces of the structure are compressed to the middle surface, and a thickness is assigned to the structure. Other than simplifying the geometry, this also

allows the option for making other simplifying assumptions, such as neglecting bending and thereby limiting the shell to membrane deformation only.

3.4 Perforated Shell Geometry

Two general perforated hemispherical shell structures were studied in this analysis. The first case studied was a hemispherical shell with a hole at the apex, as shown in Fig. 3.3. This configuration is of primary importance in the design of fusion target chambers, e.g., the apex hole is required for target injection and also maintenance. A detailed drawing of this configuration is shown in Fig. 3.4 with all associated dimensions and variables. Obviously, for hemispherical shells, the half-angle, ϕ_0, was maintained at 90°. For each thickness to shell radius ratio, *h/R*, the apex hole radius to shell radius ratio, *a/R*, was evaluated for a wide range of values.

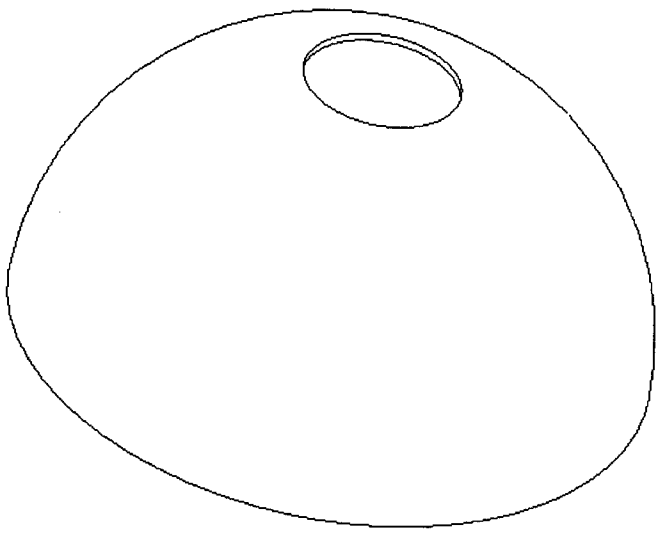

Fig. 3.3. Isometric view of a hemispherical shell with an apex hole.

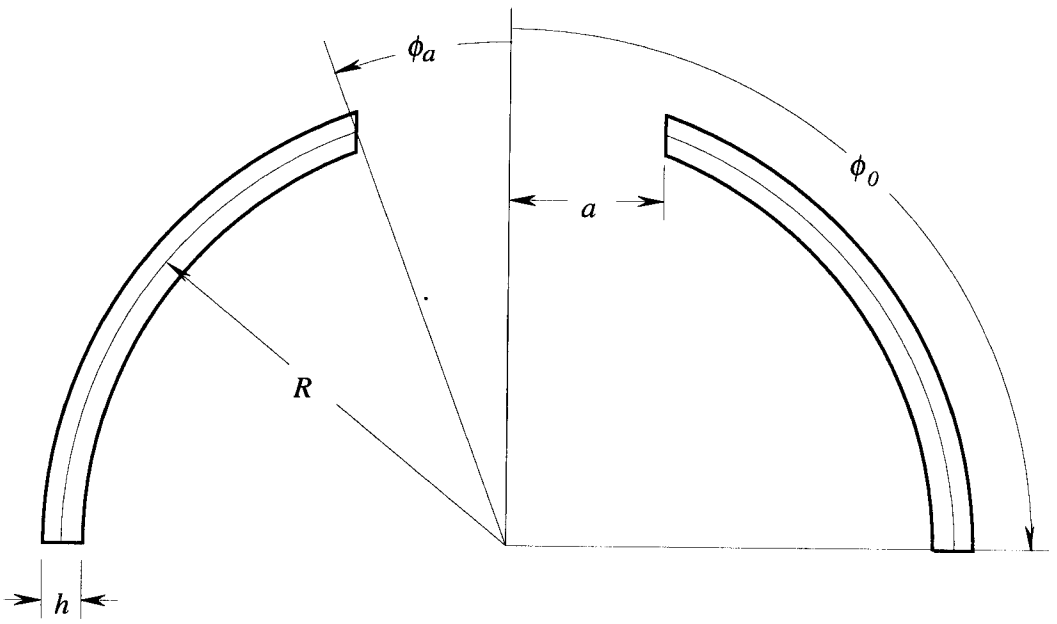

Fig. 3.4. Geometry definitions of a hemispherical shell with an apex hole.

The second hemispherical shell studied had circumferential holes in addition to the apex hole. An isometric view of this configuration is shown in Fig. 3.5. A detailed drawing is shown in Fig. 3.6. Like the previous shell, the hemispherical shell with an apex hole and circumferential holes was tested for three *h/R* values. The circumferential hole radius to shell radius ratio, *b/R*, was varied for each *h/R* ratio. The radius of the apex hole, *a*, was held constant. As a general case, the distance of the circumferential hole axis from the apex, ϕ_b, was taken as 45° for all analyses.

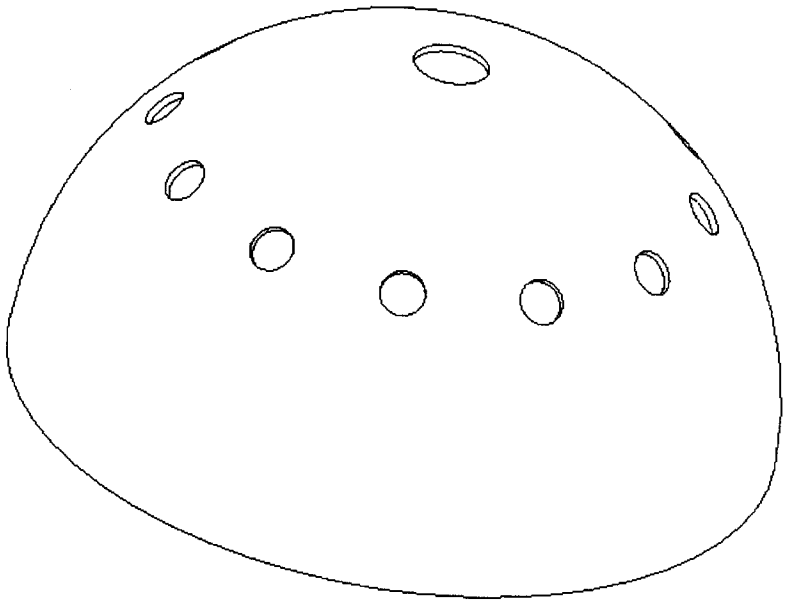

Fig. 3.5. Isometric view of a hemispherical shell with an apex hole and 12 circumferential holes.

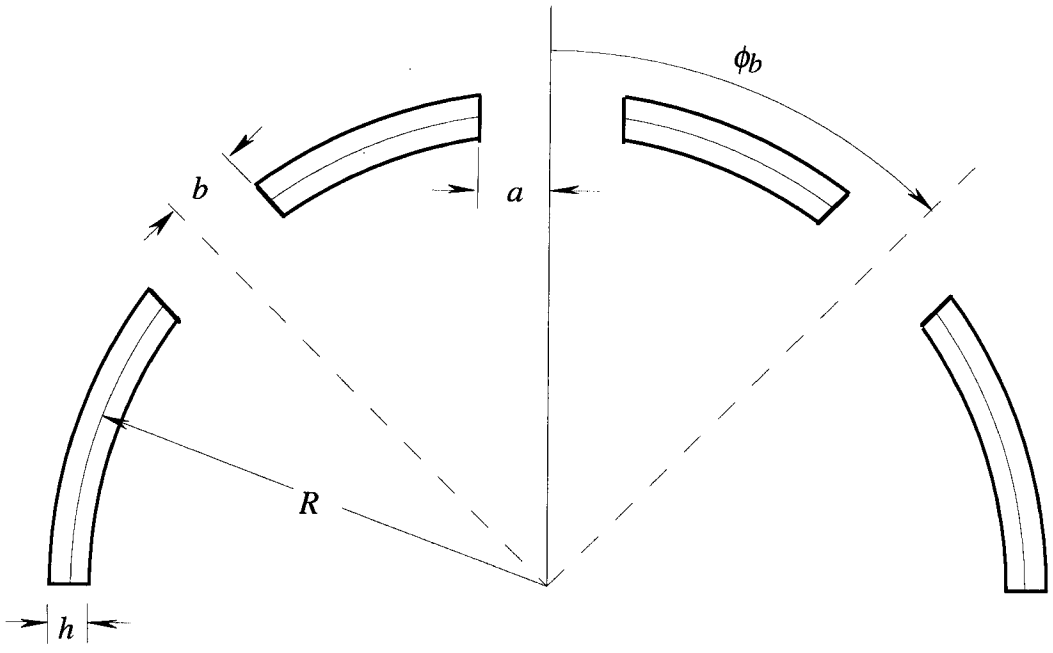

Fig. 3.6. Geometry of a hemispherical shell with an apex hole and circumferential holes.

3.5 Nondimensional Frequency Parameter

All numerical frequency results in this study will be presented in terms of the nondimensional frequency parameter [3.1], Ω, given by

$$\Omega = f 2\pi R \sqrt{\frac{\rho\left(1-\upsilon^2\right)}{E}} \tag{3.1}$$

where f is the frequency, ρ is the mass density, υ is Poisson's ratio, and E is the modulus of elasticity. Some previous studies [3.2] have used a classical nondimensional frequency parameter, Ω', which neglects the effects from Poisson's ratio and is given by

$$\Omega' = f 2\pi R \sqrt{\frac{\rho}{E}} \tag{3.2}$$

These nondimensional frequency parameters are used for the case of spherical shells with any boundary conditions and shell half angle, ϕ_0.

3.6 References

[3.1] Wilkinson, J. P., and Kalnins, A., "On Nonsymmetric Dynamic Problems of Elastic Spherical Shells," *Journal of Applied Mechanics*, Vol. 32, 1965, pp. 525-532.

[3.2] Naghdi, P. M., and Kalnins, A., " On Vibrations of Elastic Spherical Shells," *Journal of Applied Mechanics,* Vol. 29, 1962, pp. 65-72.

Chapter 4

Finite Element Model Verification

4.1 Introduction

The finite element models used in this research were created using a combination of commercially available software packages. The surface geometries of the models were created using Pro/ENGINEER®. IGES was used to transfer the surface models into PATRAN® for finite element mesh creation, and ANSYS® was subsequently used for finite element analyses. Several hemispherical shell models without perforations were generated for model verification. The vibration frequencies of these models were compared with the analytical results found in the literature.

4.2 Finite Element Types

The majority of the models used for the modal analyses in this study were created with 8-node quadratic shell elements (SHELL93 [4.1]). Because of its midside node, this element is excellent for modeling curved surfaces. It has six degrees of freedom at each node: three rotational and three translational. A schematic of this element is shown in Fig. 4.1. The element includes the effects of out-of-plane (normal) stress, transverse shear stress, transverse shear strain, and shear deformation. Transverse shear stress is assumed to be constant through the element thickness, and the out-of-plane stress varies linearly through the thickness. The element will also allow for plasticity, stress stiffening, large deflection, and large strain. The deformation shapes are quadratic in both in-plane directions [4.1].

Several axisymmetric shells were also modeled with 2-node axisymmetric elements (SHELL51 [4.2]). These elements were used to minimize computational time when identifying higher axisymmetric modes and examining impulse loading solutions. The elements were also used to verify the response of the quadratic shell element models. All hemispherical shells with circumferential holes require the use of quarter symmetry models since the shells are not axisymmetric.

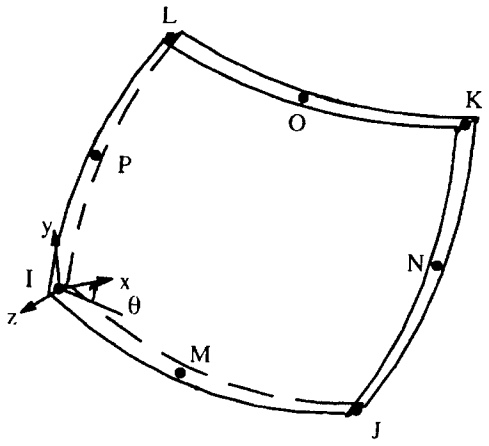

Fig. 4.1. Schematic of the 8-node shell element [4.1].

4.3 Finite Element Model Verification

Eikrem and Doige [4.3] performed an analytical and experimental analysis of the axisymmetric vibrations of a hemispherical shell with a clamped edge. Their analysis was based on the equations of motion derived by Naghdi [4.4] which neglected rotary inertia and transverse shear deformation. Their experimental and analytical results agreed well. A quarter symmetry finite element model of this shell was created and is shown in Fig. 4.2. The nondimensionalized axisymmetric frequencies of this model were compared to the analytical results of Eikrem and Doige. Table 4.1 shows that the FE results correspond within 1% of the analytical results.

Because of the boundary conditions needed to model quarter symmetry, axisymmetric torsional modes of vibration are not excited in any of the analyses. This is an acceptable simplification since only axisymmetric, radial impulse loads are of concern in this investigation, which will not excite torsional modes of vibration.

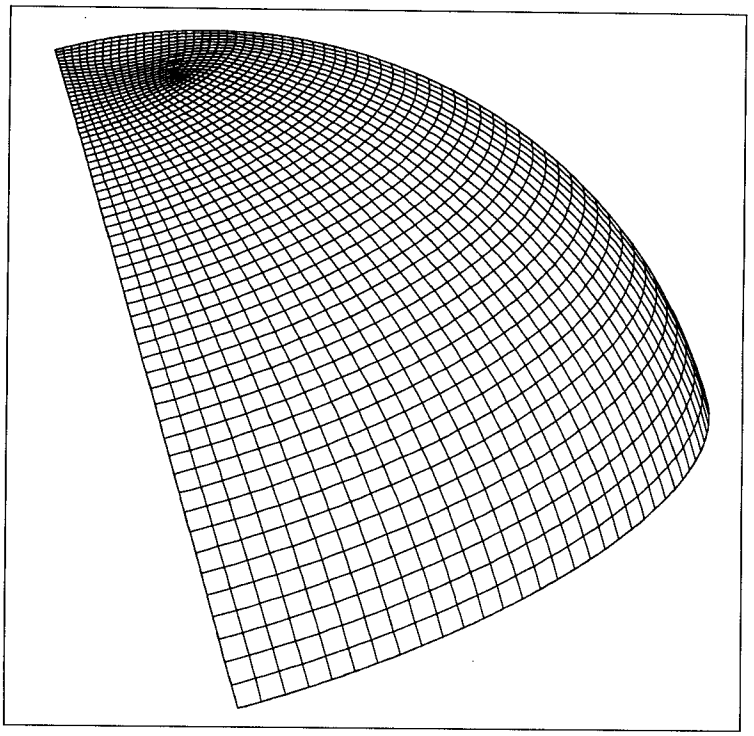

Fig. 4.2. Quarter symmetry finite element model of the hemispherical shell studied by Eikrem and Doige [4.3] (1887 elements).

Table 4.1. Nondimensional natural frequencies, Ω, of the first six axisymmetric modes of a hemispherical shell studied by Eikrem and Doige [4.3] compared with the FE results of this investigation. The shell studied had the following parameters: $h/R = 0.005$, $\upsilon = 0.3$, clamped edge.

Axisymmetric Mode Number	Eikrem & Doige Analytical Solution Ω	FE Solution Ω	Percent Difference [%]
1	0.7183	0.7189	-0.08
2	0.8891	0.8896	-0.06
3	0.9272	0.9277	-0.05
4	0.9463	0.9464	-0.01
5	0.9635	0.9639	-0.04
6	0.9854	0.9865	-0.11

The asymmetric vibrations of spherical shells were studied by De Souza and Croll [4.5] and Singh and Mirza [4.6]. De Souza and Croll based their analysis on a finite difference model formulated from classical thin shell theory, whereas the analysis of Singh and Mirza was performed using finite element models. Both studies placed a small hole at the shell apex to remove the singularities that occur in the governing equations at that point. Spherical shells ranging from a shallow cap to a hemispherical dome were studied, including clamped edge boundary conditions. For this investigation, a full model of a hemispherical shell with a clamped edge was created and is shown in Fig. 4.3. The resulting asymmetric frequencies of this model were compared to those found in the literature. As shown in Tables 4.2 and 4.3, the asymmetric frequencies agree within 1% for both sets of analytical results.

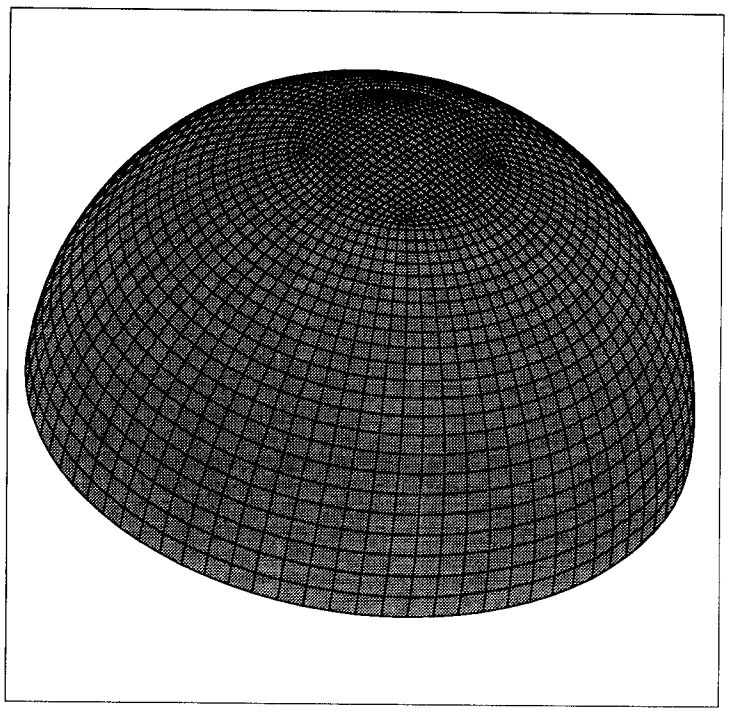

Fig. 4.3. Finite element model of the hemispherical shell studied by De Souza and Croll [4.5] and Singh and Mirza [4.6] (2480 elements).

Table 4.2. Nondimensional natural frequencies, Ω, of the first eight asymmetric modes of a hemispherical shell studied by De Souza and Croll [4.5] compared with the FE results of this investigation. The shell studied had the following parameters: $h/R = 0.005$, $\upsilon = 0.3$, clamped edge.

Asymmetric Mode - *mi* *m* = meridonal wave number *i* = circumferential wave number	De Souza & Croll Finite Difference Ω	FE Solution Ω	Percent Difference [%]
11	0.5385	0.5372	0.24
21	0.8472	0.8464	0.09
12	0.8580	0.8580	0.00
13	0.9010	0.9000	0.11
31	0.9141	0.9131	0.11
22	0.9191	0.9170	0.23
14	0.9190	0.9182	0.09
15	0.9300	0.9296	0.04

Table 4.3. Nondimensional natural frequencies, Ω, of the first eight asymmetric modes of a hemispherical shell studied by Singh and Mirza [4.6] compared with the FE results of this investigation. The shell studied had the following parameters: $h/R = 0.005$, $\upsilon = 0.3$, clamped edge.

Asymmetric Mode - *mi* *m* = meridonal wave number *i* = circumferential wave number	Singh & Mirza FE Solution Ω	FE Solution Ω	Percent Difference [%]
11	0.5394	0.5372	0.41
21	0.8477	0.8464	0.15
12	0.8585	0.8580	0.06
13	0.9004	0.9000	0.04
31	0.9139	0.9131	0.09
22	0.9174	0.9170	0.04
14	0.9187	0.9182	0.05
15	0.9301	0.9296	0.05

4.4 Mesh Refinement

An investigation was performed to identify the minimum number of elements needed to generate accurate results in a modal analysis. The fundamental axisymmetric frequency of a uniform hemispherical shell (h/R = 0.005) analytically determined by Eikrem and Doige [4.3] was used as a target value (f = 4848.9 Hz). Both 8-node quadratic shell elements and 2-node axisymmetric elements were studied. Figure 4.4 shows the frequency computed using the FE method as a function of the number of quadratic shell elements; Fig. 4.5 shows the FE frequency as a function of the number of 2-node axisymmetric elements. As shown, the models require relatively few elements to generate accurate results. The model created with quadratic elements converged to a frequency within 1% of the target value with approximately 500 elements. The frequency of the shell created with the axisymmetric elements converged to within 1% of the target value with only 30 elements.

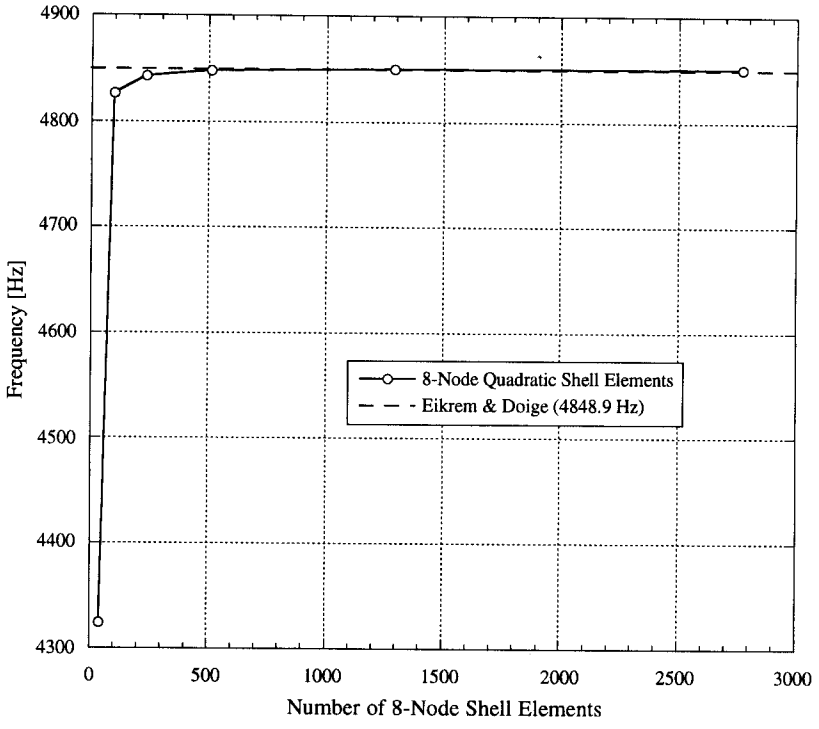

Fig. 4.4. Finite element frequency of the fundamental axisymmetric mode for a hemispherical shell with a clamped edge (h/R = 0.005) as a function of the number of 8-node quadratic shell elements used.

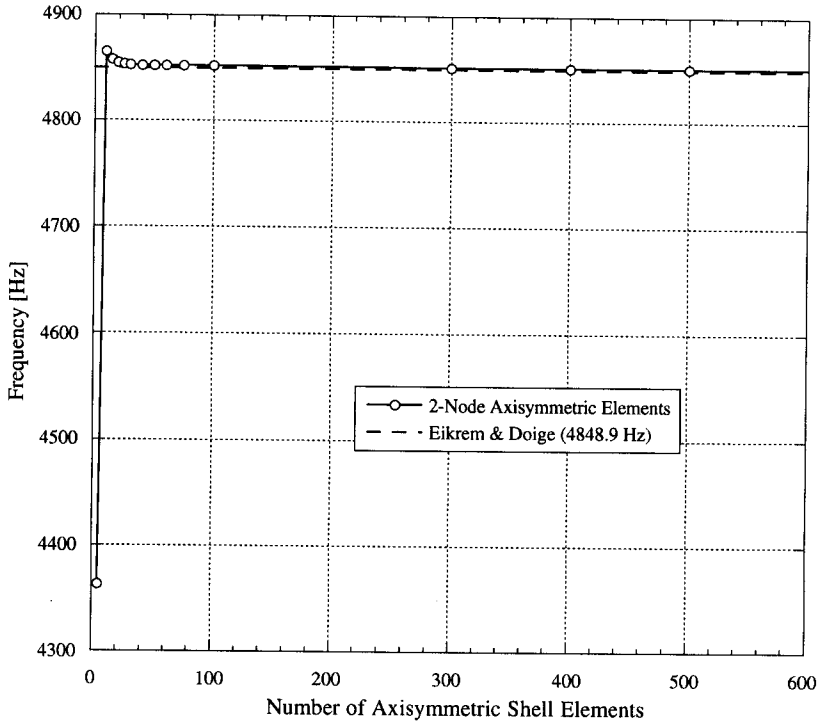

Fig. 4.5. Finite element frequency of the fundamental axisymmetric mode for a hemispherical shell with a clamped edge (h/R = 0.005) as a function of the number of 2-node axisymmetric elements used.

4.5 References

[4.1] ANSYS User's Manual for Revision 5.3, Vol. 3, pp. 4-643-4-649.

[4.2] ANSYS User's Manual for Revision 5.3, Vol. 3, pp. 4-351-4-357.

[4.3] Eikrem, A. K. A., and Doige, A. G., "Natural Frequencies of a Hemispherical Shell," *Experimental Mechanics*, Vol. 12, No. 12, 1972, pp. 575-579.

[4.4] Naghdi, P. M., "On the Theory of Thin Elastic Shells," *Quarterly of Applied Mathematics*, Vol. 14, 1957, pp. 369-380.

[4.5] De Souza, V. C., and Croll, J. G. A., "An Energy Analysis of the Free Vibrations of Isotropic Spherical Shells," *The Journal of Sound and Vibration*, Vol. 73, No. 3, 1980, pp. 379-404.

[4.6] Singh, A. V., and Mirza, S., "Asymmetric Modes and Associated Eigenvalues for Spherical Shells," *The Journal of Pressure Vessel Technology*, Vol. 107, 1985, pp. 77-82.

Chapter 5

Axisymmetric Vibrations of a Hemispherical Shell with an Apex Hole

5.1 Introduction

In 1992 and 1993, Hwang and Foster [5.1, 5.2] presented an analytical and finite element analysis of the axisymmetric vibrations of a shallow spherical shell with an apex hole. No known study has been performed on the dynamic behavior of deep spherical shells with perforations. The simplest perforation pattern, and most important pattern in fusion applications, is an axisymmetric shell with a single apex hole.

Any fusion target chamber with a hemispherical endcap will most likely have an apex hole for target insertion and maintenance. This chapter presents numerical results for the axisymmetric frequencies of the first three modes of clamped hemispherical shells with apex hole radius to shell radius ratios, a/R, varying from 0 to 0.8. Shells with thickness-to-radius ratios, h/R, of 0.005, 0.010, and 0.050 were evaluated.

5.2 Finite Element Model

Because this research had a direct application, analyses were performed to represent conditions anticipated in a fusion target chamber. When a uniform, radial, impulse load is applied to an axisymmetric shell, only the axisymmetric modes will be excited. Also, when a hemispherical shell is used as a structural component of a target chamber, the edge will most likely be rigidly clamped. Therefore, only the axisymmetric natural frequencies of a hemispherical shell with a clamped edge were studied. Modeling using symmetry conditions can minimize computational time and allow proper mesh refinement. Quarter symmetry models were used to study the axisymmetric case of a hemispherical shell with an apex hole. An example of the mesh used is shown in Fig. 5.1. Symmetry conditions ($u = w_{,\phi} = \beta_\phi = 0$) were applied to the edges at $\theta = 0°$ and $\theta = 90°$. The bottom edge at $\phi = 90°$ was rigidly clamped ($u = v = w = w_{,\phi} = \beta_\phi = \beta_\theta = 0$). A quarter symmetry model was used rather than a model created from axisymmetric elements since quarter symmetry was required to model the non-axisymmetric circumferential perforation pattern.

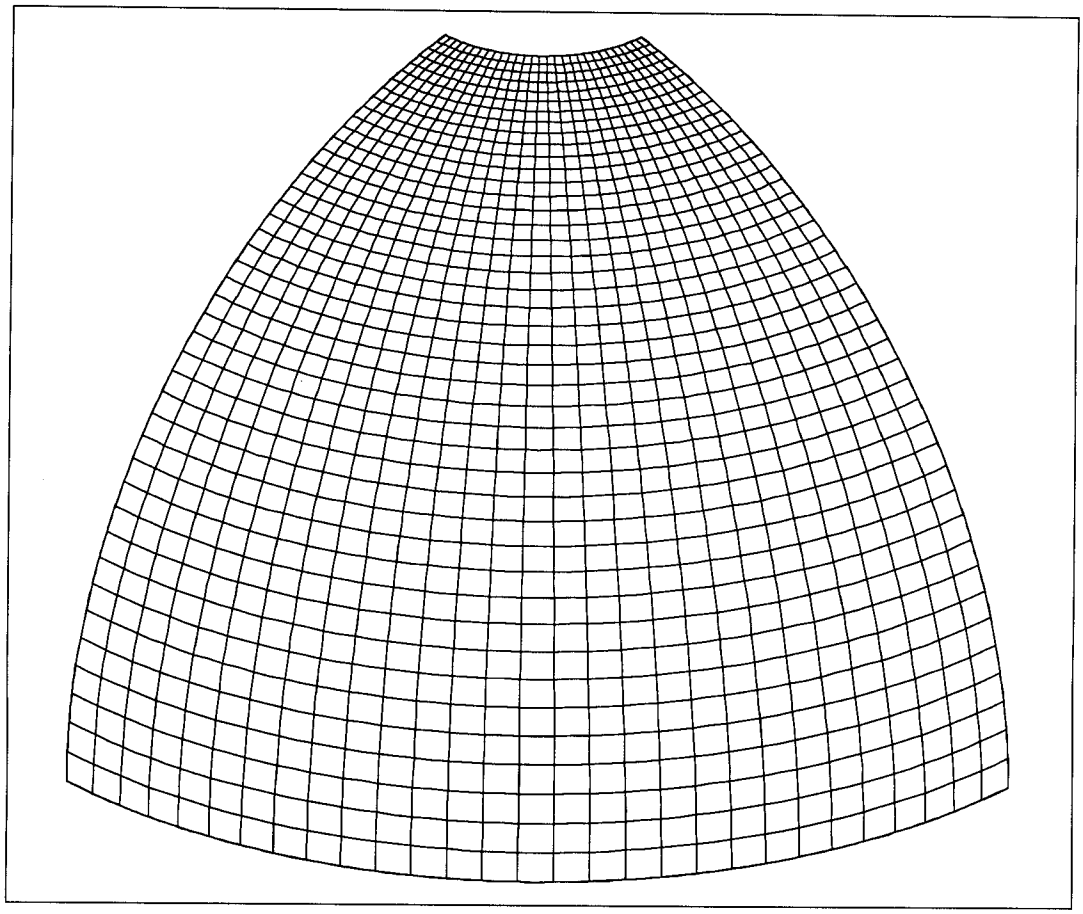

Fig. 5.1. Quarter symmetry finite element model of a hemispherical shell with an apex hole (1247 elements).

5.3 Axisymmetric Vibration Natural Frequencies

The analyses were performed to identify the first three axisymmetric modes of each hemispherical shell investigated. An example of fundamental axisymmetric frequency of the finite element model is shown in Fig. 5.2. Figure 5.3 shows Ω vs. a/R for the first axisymmetric mode for each h/R ratio evaluated. As shown, Ω increases as a/R increases. Interestingly, the apex hole has negligible effects on the natural frequency for small radius values. The percent increase in Ω with increasing a/R is shown in Fig. 5.4. The nondimensional frequency, Ω, increased less than 1% until the apex-hole

radius to shell radius ratio, a/R, was approximately 0.15. This is shown to be true for each h/R value tested.

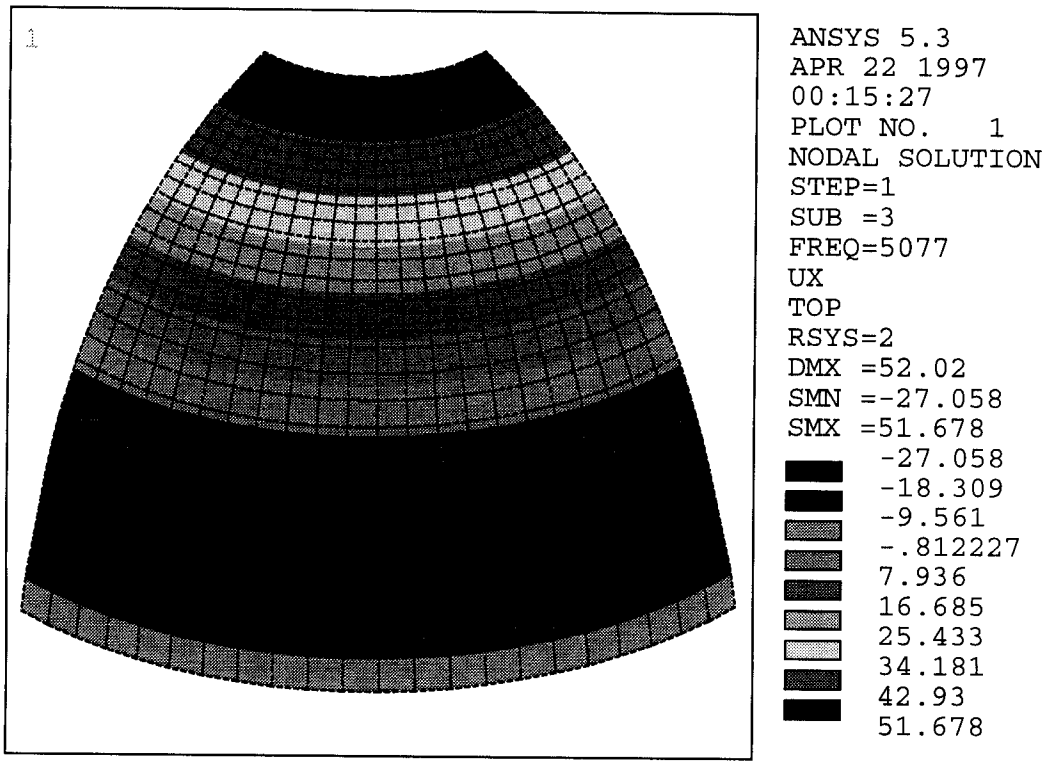

Fig. 5.2. Fundamental axisymmetric mode of a finite element hemispherical shell with an apex hole and the following parameters: $\Omega = 0.7522$, $R = 5.0$ in., $h = 0.050$ in., $a = 1.50$ in., $E = 30.0\times10^6$ psi, $\rho = 0.733\times10^{-3}$ lb-s^2/in^4, $\upsilon = 0.3$, 638 elements.

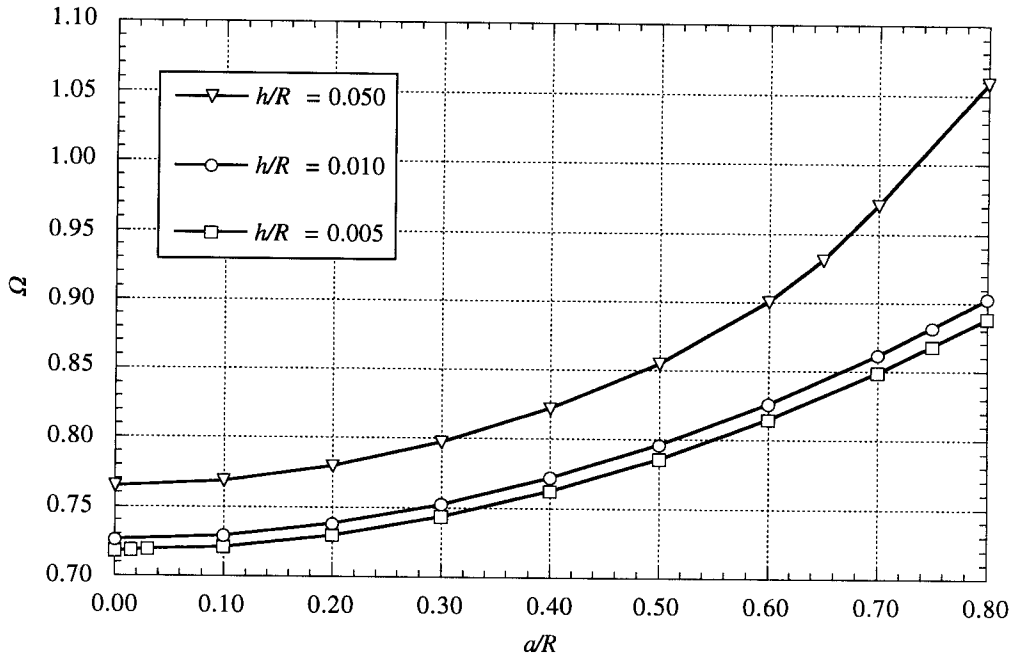

Fig. 5.3. Nondimensional frequencies of the first axisymmetric mode for three *h/R* ratios.

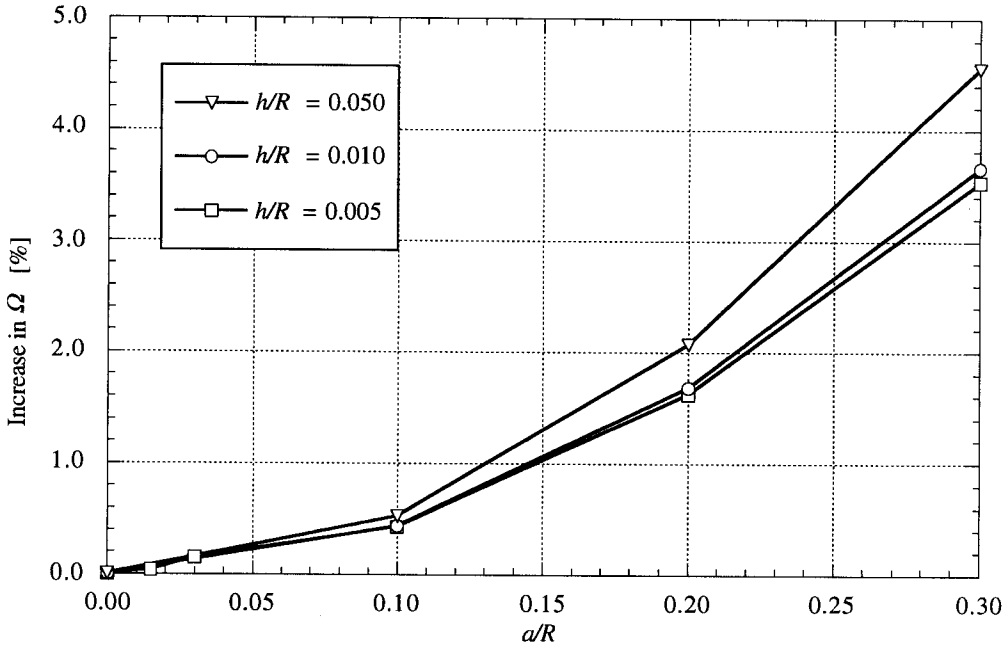

Fig. 5.4. Percent increase in the nondimensional frequency of the first axisymmetric mode for three *h/R* ratios.

Figures 5.5 through 5.7 present Ω for the first three axisymmetric modes for each h/R value. For the thinnest shell tested (Fig. 5.5, $h/R = 0.005$), Ω increased with increases in a/R, for all three modes. For the shell with $h/R = 0.010$ (Fig. 5.6), the third axisymmetric mode deviated from the expected path, i.e., at $a/R \approx 0.75$, Ω began to decrease. As shown in Fig. 5.7, both the second and third axisymmetric modes followed unexpected paths for the thickest shell tested ($h/R = 0.050$). The normalized mode shapes of the fundamental axisymmetric modes for a hemispherical shell with $h/R = 0.050$ with an apex hole are shown in Fig. 5.8.

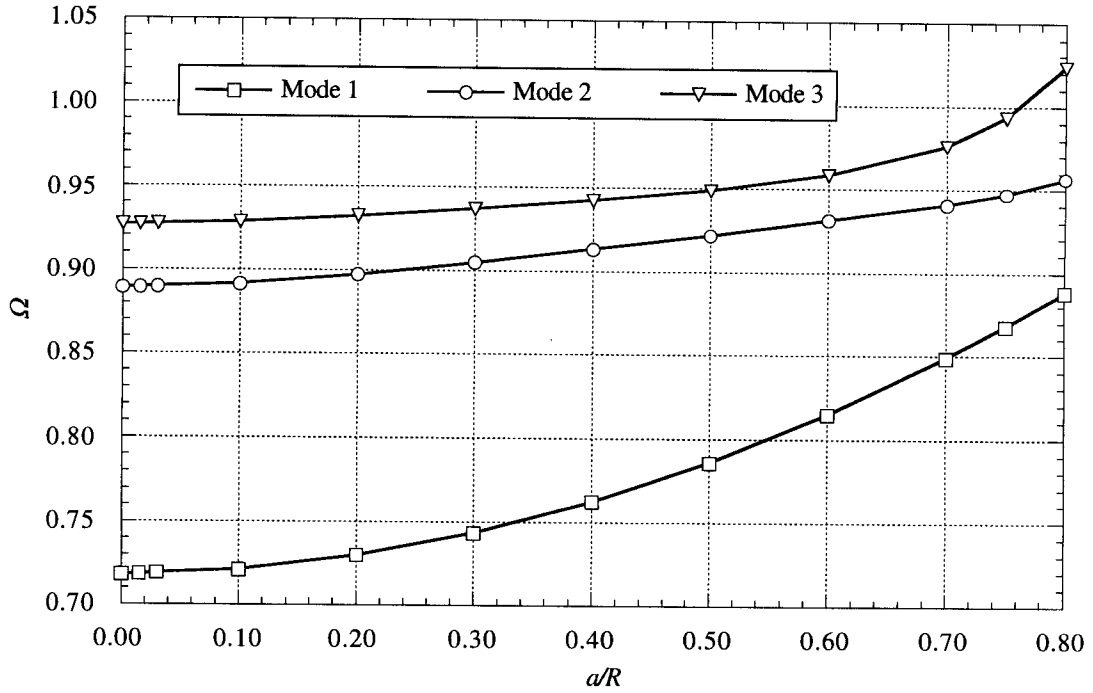

Fig. 5.5. Nondimensional frequencies for the first three axisymmetric modes ($h/R = 0.005$).

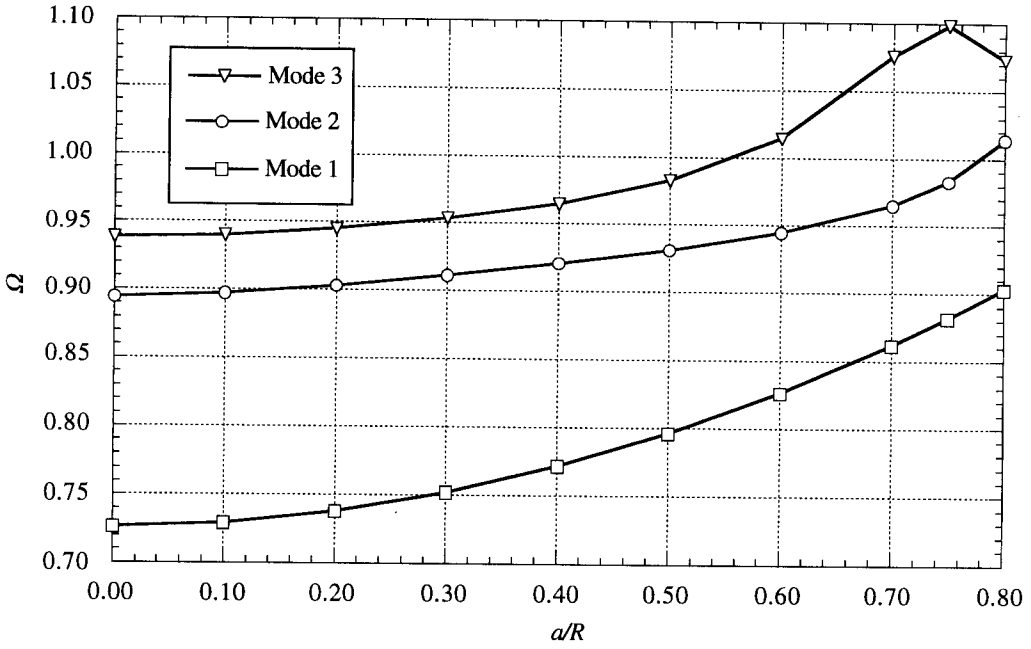

Fig. 5.6. Nondimensional frequencies for the first three axisymmetric modes ($h/R = 0.010$).

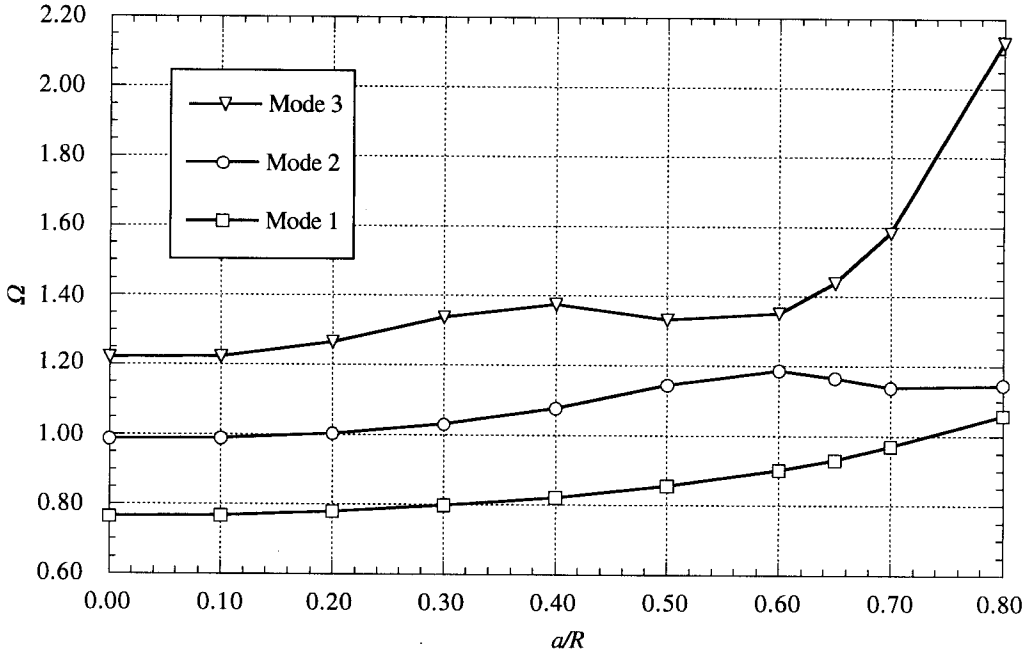

Fig. 5.7. Nondimensional frequencies for the first three axisymmetric modes ($h/R = 0.050$).

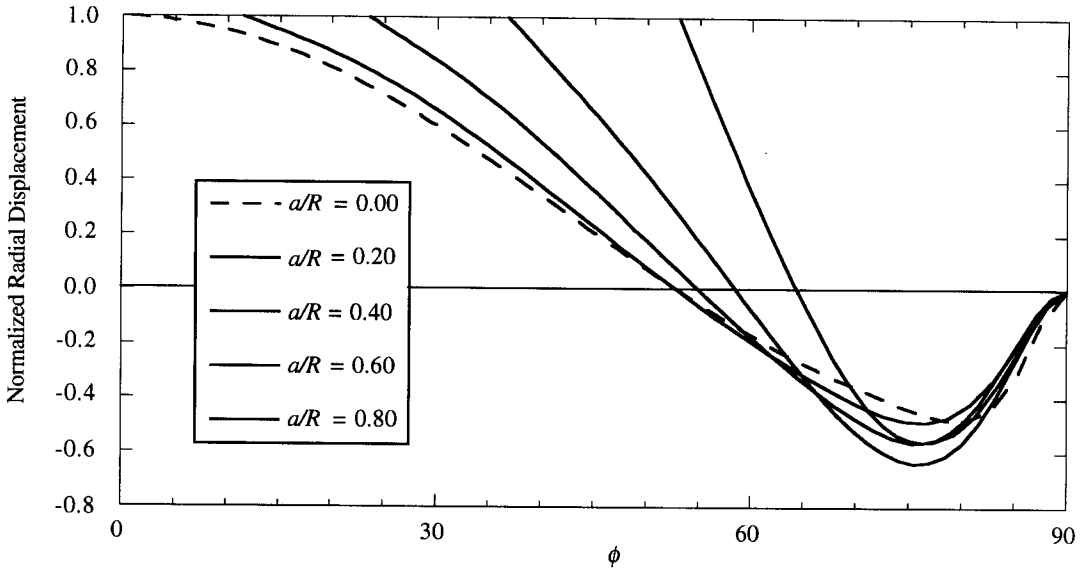

Fig. 5.8. Normalized mode shapes of the fundamental axisymmetric mode for a clamped hemispherical shell with an apex hole ($h/R = 0.050$).

5.4 References

[5.1] Hwang, D. Y., and Foster, W. A., Jr., "Analysis of Axisymmetric Free Vibration of Isotropic Shallow Spherical Shells with a Circular Hole," *Journal of Sound and Vibration*, Vol. 157, No. 2, 1992, pp. 331-343.

[5.2] Hwang, D. Y., and Foster, W. A., Jr., "Axisymmetric Free Vibration of Shallow Spherical Shells with a Circular Rigid Insert," *Journal of Pressure Vessel Technology*, Vol. 115, 1993, pp. 207-209.

Chapter 6

Axisymmetric Impulse Loading of a Hemispherical Shell with an Apex Hole

6.1 Impulse Loading of a Uniform Hemispherical Shell

Originally, it was assumed that applying a uniform radial impulsive pressure load to a hemispherical shell would result in the first fundamental axisymmetric mode being the largest contributor to displacement. To confirm this response, a clamped edge hemispherical shell without perforations was modeled with axisymmetric elements and subjected to a uniform radial pressure of 450 psi for 2.0×10^{-6} seconds (see Fig. 6.1). The use of axisymmetric elements minimizes the amount of computational time needed for extended transient analyses. The computations reported in this chapter were carried out to 0.008 seconds. Since this research is primarily interested in the natural frequencies of hemispherical shells, damping was neglected in all studies. This chapter is limited to the case of a perforated hemispherical shell with a h/R ratio of 0.010. The resulting time-dependent radial displacement of a FE node point at approximately ϕ = 40° is shown in Fig. 6.2 to $t = 0.0025$ seconds. From the modal analysis in Chapter 5, it is known that the fundamental axisymmetric frequency for the shell with h/R = 0.010 is 4900 Hz ($\Omega = 0.726$). The response of the shell to the impulse loading was indeed axisymmetric, but the primary response frequency appeared much higher than the fundamental frequency.

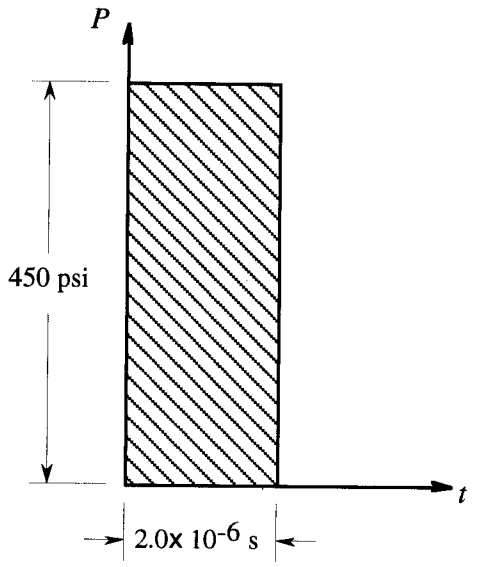

Fig. 6.1. Impulse load magnitude and duration.

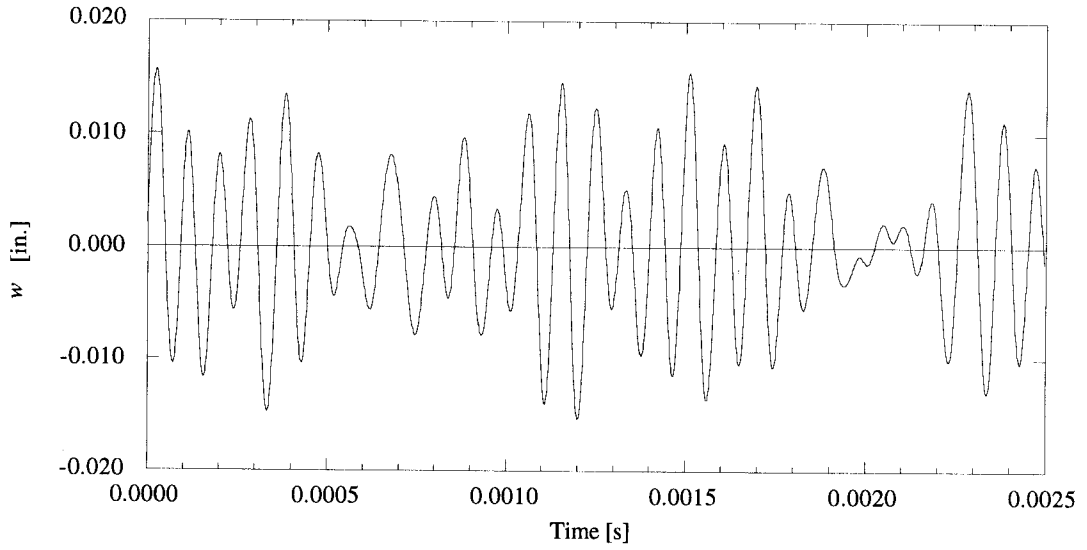

Fig. 6.2. Radial impulse response of a node at $\phi \approx 40°$ on a uniform hemispherical shell. The shell tested had the following parameters: $R = 5.0$ in., $h = 0.050$ in., $a = 0.0$ in., $E = 30.0\times10^6$ psi, $\rho = 0.733\times10^{-3}$ lb-s^2/in^4, $\upsilon = 0.3$.

As shown by Fig. 6.2, the response was not uniform over time. The variation in radial displacement was caused by traveling wave effects. To find what modes were

contributing most to the displacements, a Fourier transform was performed on the data using Mathematica®. This method identified the approximate contributions of individual modes. As shown in Fig. 6.3, the main contributions to displacement are from modes other than the first three studied in Chapter 5. A modal analysis of the shell was extended to identify the exact frequencies of the first 13 axisymmetric modes. The resulting nondimensional axisymmetric frequencies are shown in Table 6.1. According to Fig. 6.3 and Table 6.1, the main contributors to displacement are the tenth ($\Omega = 1.584$) and eleventh axisymmetric modes ($\Omega = 1.693$).

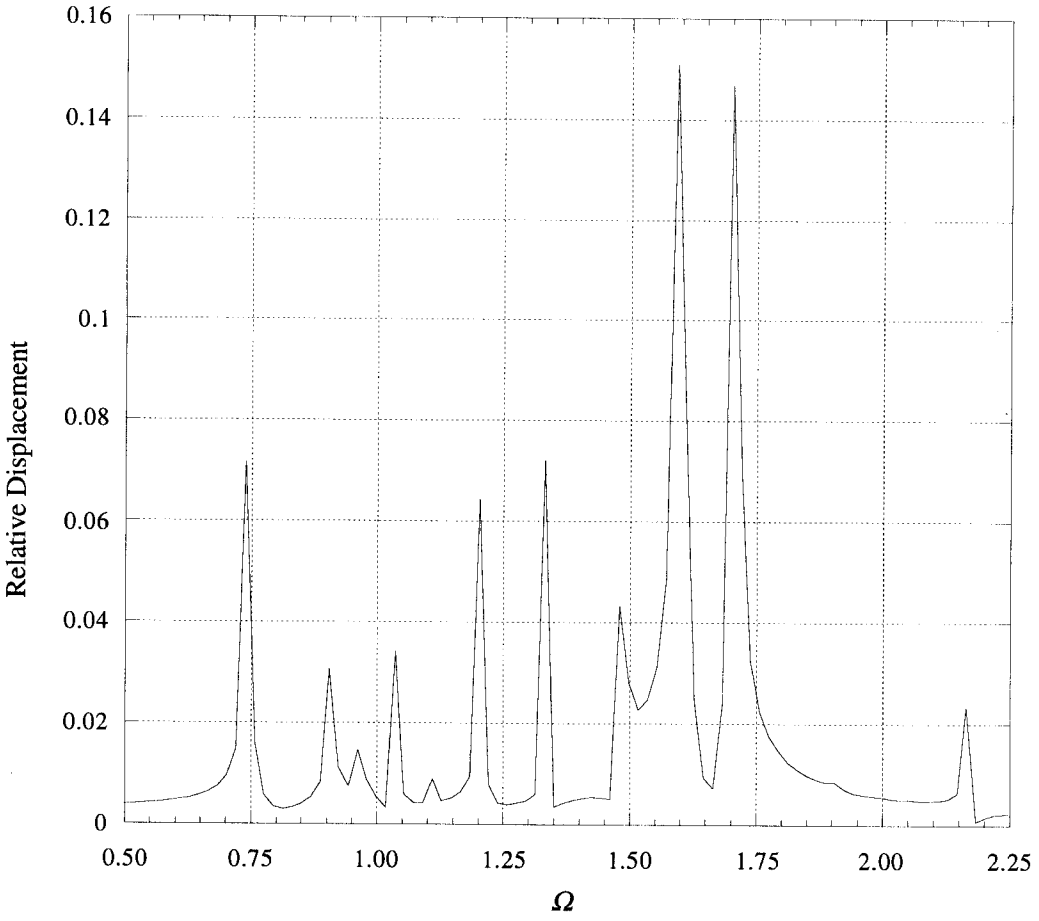

Fig. 6.3. Fourier transform of the data shown in Fig. 6.2 (uniform hemispherical shell with $h/R = 0.010$). Frequency values are shown in nondimensional terms.

Table 6.1. Nondimensional frequencies for the first 13 axisymmetric modes of a uniform hemispherical shell with a clamped edge ($h/R = 0.010$).

Axisymmetric Mode	Ω
1	0.7263
2	0.8948
3	0.9382
4	0.9731
5	1.0209
6	1.0909
7	1.1884
8	1.3157
9	1.4688
10	1.5837
11	1.6932
12	1.9061
13	2.1566

6.2 Impulse Loading of a Hemispherical Shell with an Apex Hole

Since this research was performed to aid in the design of fusion target chambers, the dynamic response of the shell to an impulse pressure is of primary importance. The previous section demonstrated that the response of a clamped unperforated hemispherical shell to a uniform radial impulse load will be dominated by contributions of modes other than the fundamental. Therefore, the study of the dynamic behavior of hemispherical shells with an apex hole was continued to find the actual response to an impulse loading.

This section studies the impulse response of two representative cases of hemispherical shells with an apex hole and clamped edges. The investigation was performed for shells with a/R values of 0.20 and 0.50. A h/R ratio of 0.010 was used for both cases. The impulse loading (shown in Fig. 6.1) was applied to both shells with the effects of damping neglected. Figures 6.4 and 6.5 show the resulting radial displacements for $a/R = 0.20$ and $a/R = 0.50$, respectively.

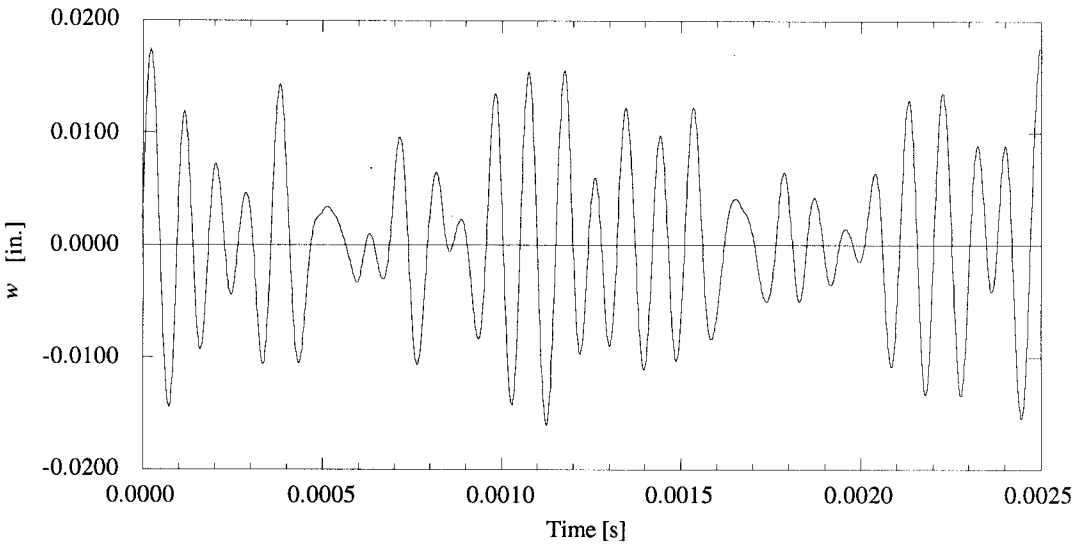

Fig. 6.4. Radial impulse response of a node at $\phi \approx 51°$ on a hemispherical shell with the following parameters: R = 5.0 in., h = 0.050 in., a = 1.0 in., E = 30.0×10^6 psi, ρ = 0.733×10^{-3} lb-s^2/in^4, υ = 0.3.

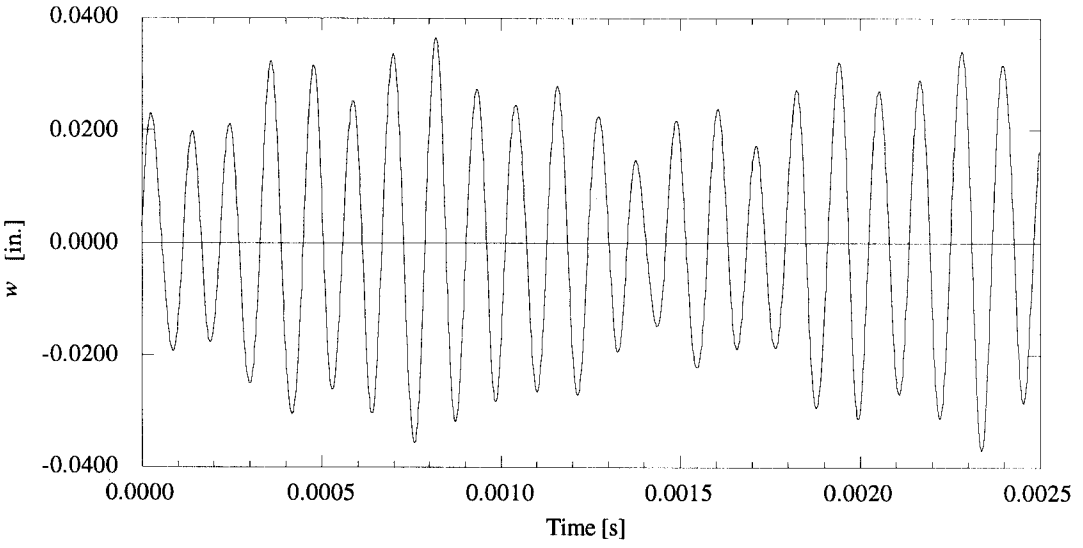

Fig. 6.5. Radial impulse response of a node at $\phi \approx 60°$ on a hemispherical shell with the following parameters: R = 5.0 in., h = 0.050 in., a = 2.5 in., E = 30.0×10^6 psi, ρ = 0.733×10^{-3} lb-s^2/in^4, υ = 0.3.

Like the previous section, a Fourier transform was performed on the radial response data for both shells. Figures 6.6 and 6.7 show the Fourier transform for $a/R = 0.20$ and $a/R = 0.05$, respectively. As with the uniform shell, contributions to displacement came from modes other than the fundamental. Modal analyses were extended for both shells to identify the frequencies of the first 11 axisymmetric modes. The nondimensional frequencies are shown in Table 6.2 for both shells studied.

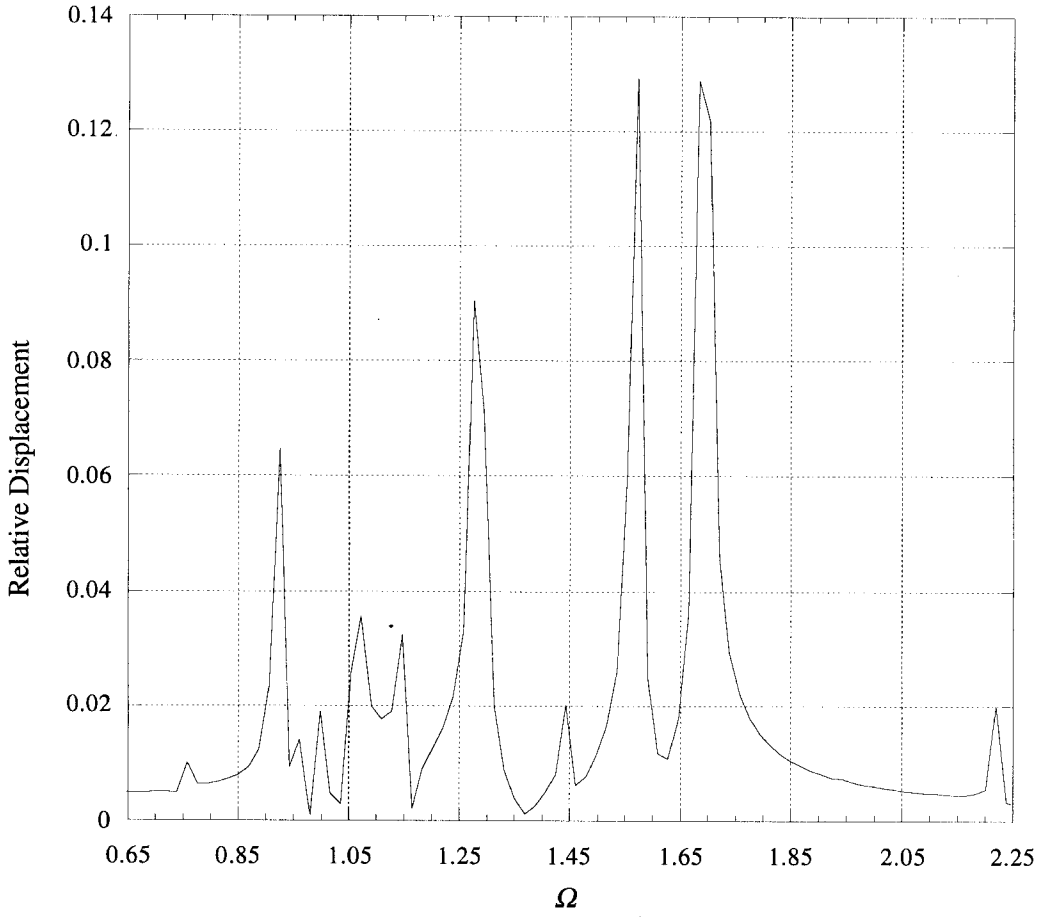

Fig. 6.6. Fourier transform of the data shown in Fig. 6.4 (hemispherical shell with $a/R = 0.2$ and $h/R = 0.010$). Frequency values are shown in nondimensional terms.

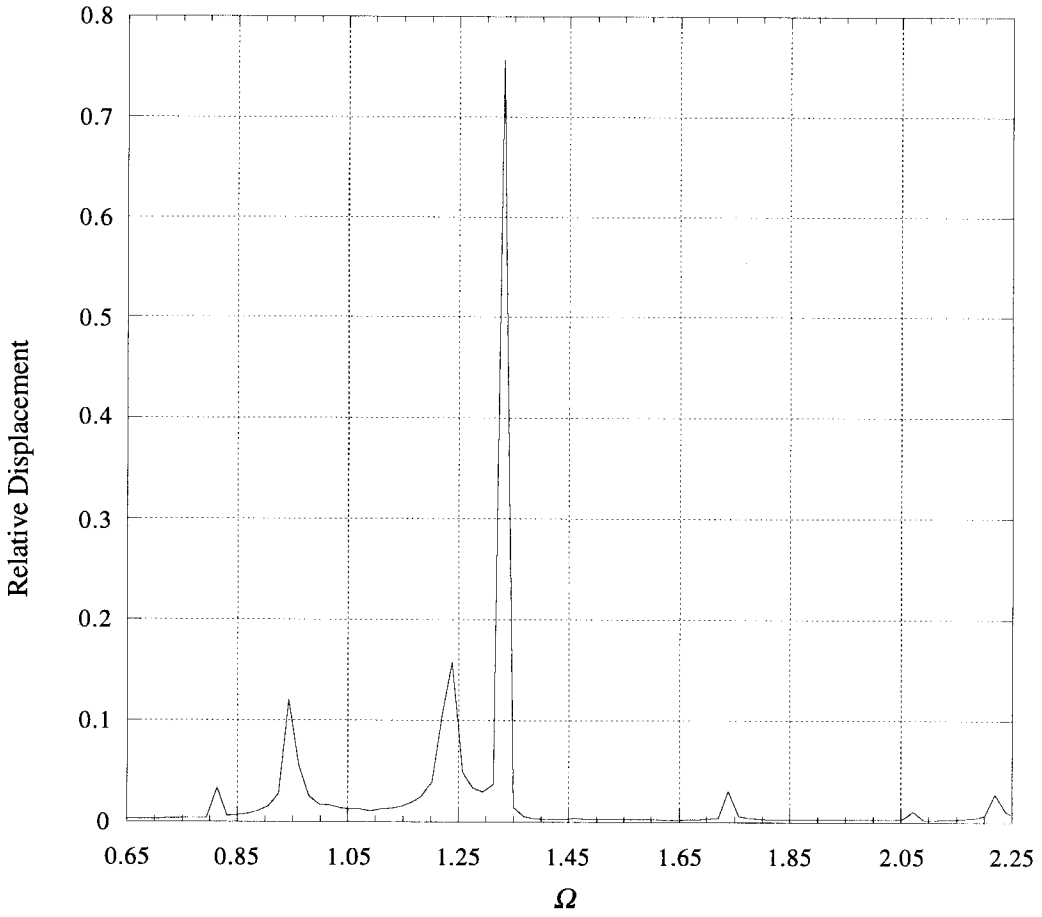

Fig. 6.7. Fourier transform of the data shown in Fig. 6.5 (hemispherical shell with a/R = 0.5 and h/R = 0.010). Frequency values are shown in nondimensional terms.

Table 6.2. Nondimensional frequencies for the first 11 axisymmetric modes of two hemispherical shells with a/R values of 0.20 and 0.50 (h/R = 0.010).

Axisymmetric Mode	Ω a/R = 0.20	Ω a/R = 0.50
1	0.7383	0.7964
2	0.9037	0.9320
3	0.9454	0.9836
4	0.9848	1.0707
5	1.0457	1.2156
6	1.1385	1.3157
7	1.2692	1.4443
8	1.4346	1.7274
9	1.5523	2.0628
10	1.6779	2.2148
11	1.9247	2.5297

Figure 6.6 shows that the main contributions to displacement are coming from the ninth (Ω = 1.552) and tenth (Ω = 1.668) axisymmetric modes for the shell with a/R = 0.20. This response is very similar to that of the uniform hemispherical shell which had displacements dominated by the tenth (Ω = 1.583) and eleventh modes (Ω = 1.693). There is only a 2.0% difference between the frequency of the ninth mode of the shell with an apex hole and the tenth mode of the uniform shell. Likewise, there is only a 1.5% difference between the frequency of the tenth mode of the shell with an apex hole and the frequency of the eleventh mode of the uniform hemispherical shell. This indicates that the response behavior of a hemispherical shell with a relatively small apex hole can be accurately approximated as a uniform shell. For a shell with a/R = 0.50, the contributions to displacement are dominated by the sixth axisymmetric mode (Ω = 1.316) as shown by Fig. 6.7. This is considerably less than that for a uniform shell.

Chapter 7

Impulse Loading of a Hemispherical Shell with Apex and Circumferential Holes

7.1 Introduction

Hemispherical shells used for fusion target chambers may have circumferential holes in addition to the apex hole. Circumferential holes are used for diagnostic equipment and laser ports. The apex hole is still needed for target insertion and maintenance. Because of the circumferential holes, the shell is no longer axisymmetric and will therefore not have axisymmetric mode shapes. This chapter investigates the response of a clamped edge hemispherical shell with 16 equally spaced circumferential holes in addition to an apex hole for the impulse load discussed in Chapter 6.

7.2 Finite Element Model

Figure 7.1 shows the quarter symmetry finite element model used for this investigation. It as 2536 nodes and 783 elements. The shell had the following parameters: R = 5.0 in., h = 0.050 in., a = 0.50 in., b = 0.25 in., $E = 30.0\times10^6$ psi, $\rho = 0.733\times10^{-3}$ lb-s^2/in^4, $\upsilon = 0.3$, $\phi_b = 45°$. The boundaries around the holes are free (not reinforced or supported).

7.3 Response to a Uniform, Axisymmetric, Impulse Load

A radial impulse pressure of 450 psi was applied for 2.0×10^{-6} seconds to the FE model shown in Fig. 7.1. The response of the shell was taken to 0.008 seconds with damping neglected. Figures 7.2 through 7.3 show the resulting shell displacements at 0.0005, 0.0010, and 0.00015 seconds, respectively. The shell deformed in approximately an axisymmetric manner at all times. Figure 7.5 shows the displacements of a node at $\phi \approx 50°$ as a function of time. A Fourier transform of the data is shown in Fig. 7.6. A modal analysis was performed to identify the frequencies of the quasi-axisymmetric modes. The resulting nondimensional frequencies are shown in Table 7.1.

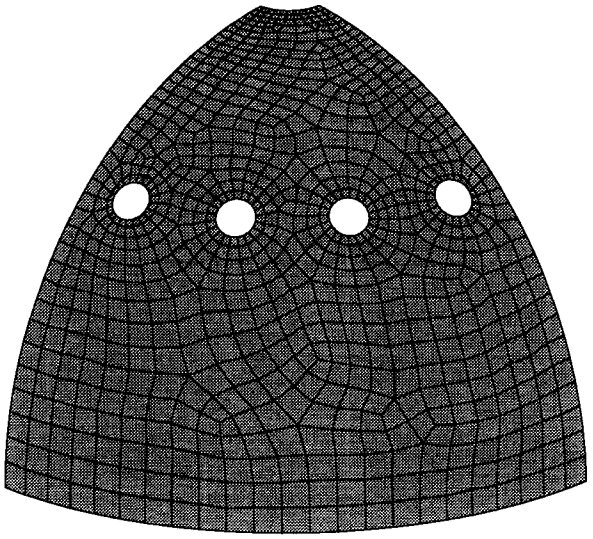

Fig. 7.1. Quarter symmetry finite element model of a hemispherical shell with 16 circumferential holes and an apex hole. The geometry has the following parameters: $a/R = 0.10$, $b/R = 0.05$, $\phi_b = 45°$, 783 elements.

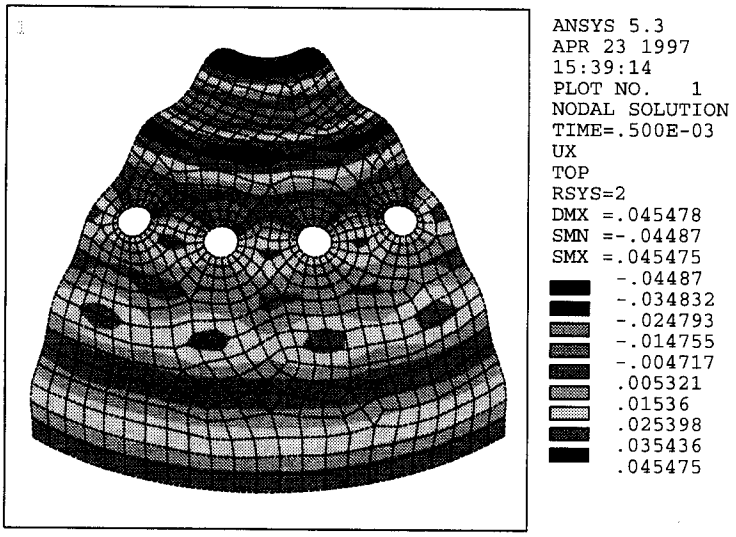

Fig. 7.2. Radial response of a perforated hemispherical shell to an impulse load at $t = 0.0005$ s. The shell had a clamped edge and the following parameters: $R = 5.0$ in., $h = 0.050$ in., $a = 0.50$ in., $b = 0.25$ in., $E = 30.0\times10^6$ psi, $\rho = 0.733\times10^{-3}$ lb-s^2/in^4, $\upsilon = 0.3$, $\phi_b = 45°$.

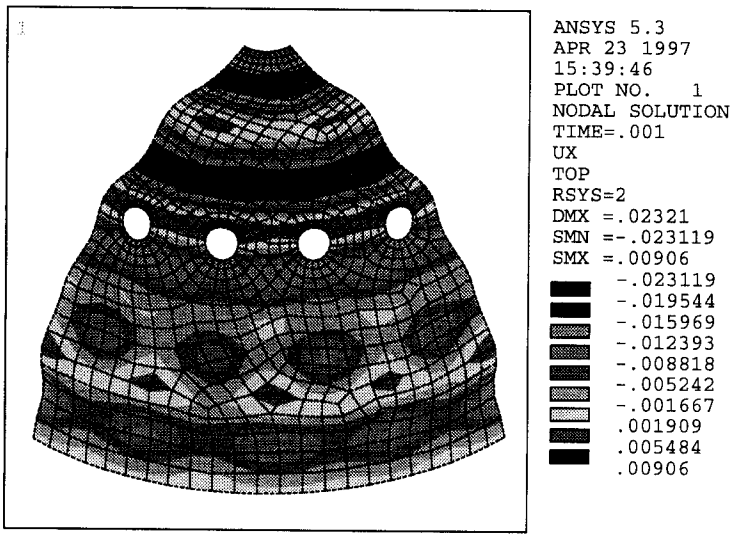

Fig. 7.3. Radial response of a perforated hemispherical shell to an impulse load at $t = 0.0010$ s. The shell had a clamped edge and the following parameters: $R = 5.0$ in., $h = 0.050$ in., $a = 0.50$ in., $b = 0.25$ in., $E = 30.0\times10^6$ psi, $\rho = 0.733\times10^{-3}$ lb-s^2/in^4, $\upsilon = 0.3$, $\phi_b = 45°$.

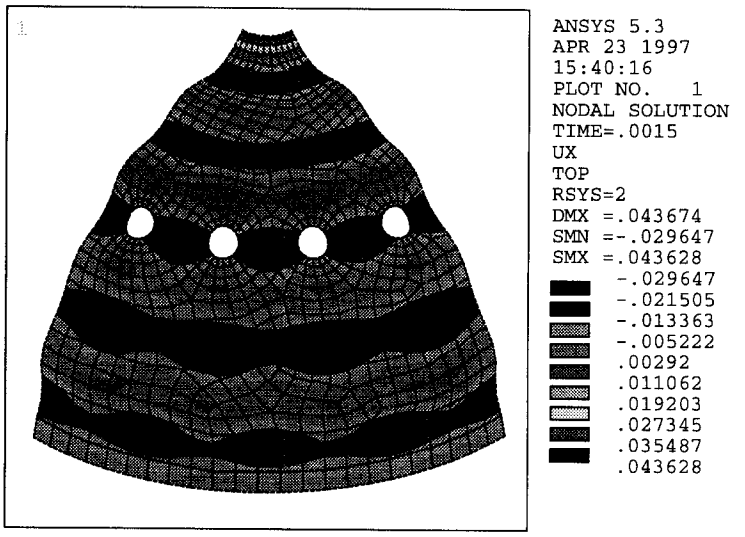

Fig. 7.4. Radial response of a perforated hemispherical shell to an impulse load at $t = 0.0015$ s. The shell had a clamped edge and the following parameters: $R = 5.0$ in., $h = 0.050$ in., $a = 0.50$ in., $b = 0.25$ in., $E = 30.0\times10^6$ psi, $\rho = 0.733\times10^{-3}$ lb-s^2/in^4, $\upsilon = 0.3$, $\phi_b = 45°$.

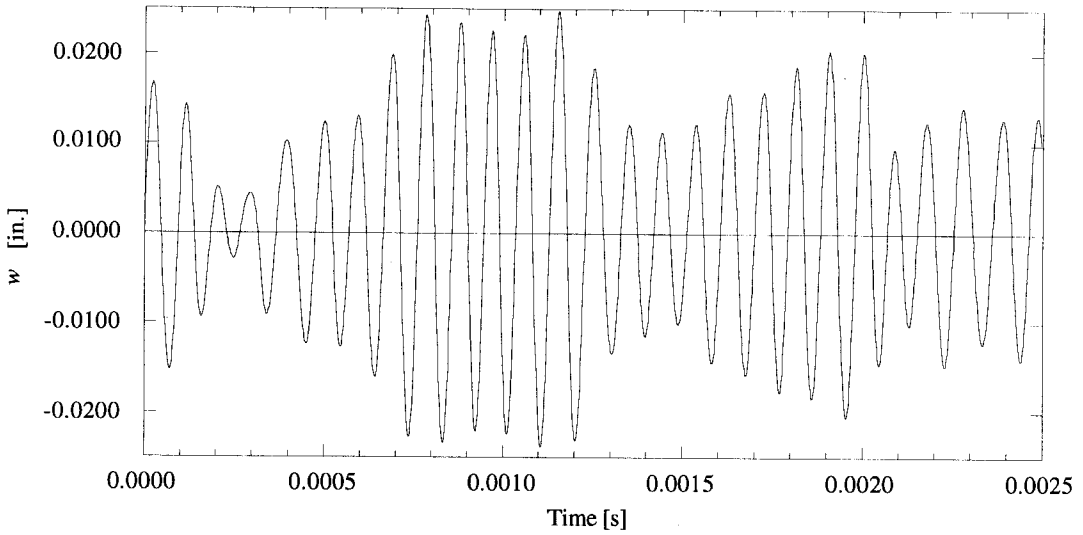

Fig. 7.5. Radial displacement of a FE node at $\phi \approx 50°$ as a function of time after an impulse load of 450 psi for 2.0×10^{-6}s.

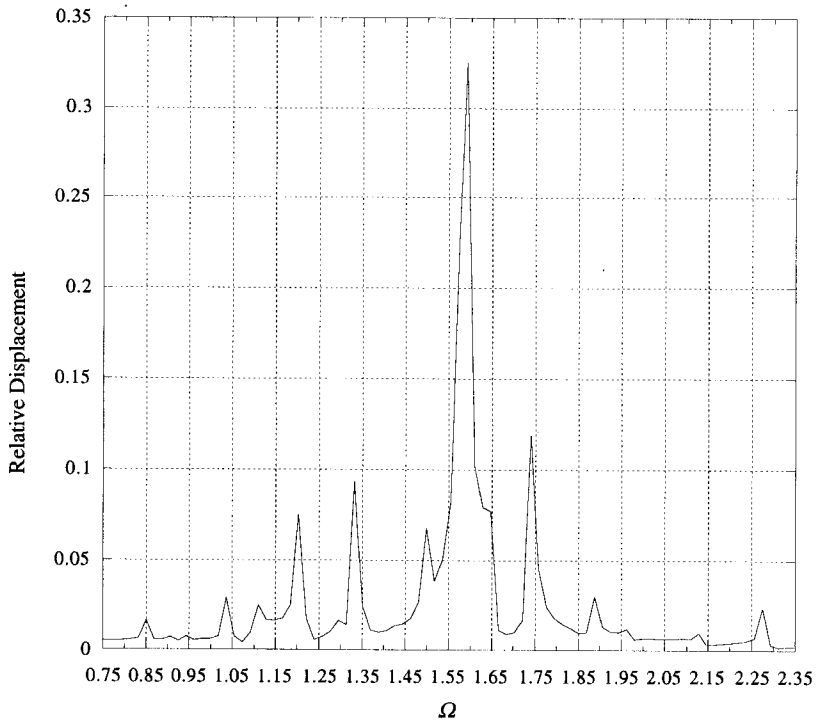

Fig. 7.6. Fourier transform of the data shown in Fig. 7.5.

Table 7.1. Nondimensional quasi-axisymmetric natural frequencies for clamped edge hemispherical shell with the following parameters: $a/R = 0.10$, $b/R = 0.05$, $h/R = 0.01$, $\phi_b = 45°$.

Quasi - Axisymmetric Mode	Ω
1	0.7073
2	0.8306
3	0.9341
4	0.9583
5	1.0149
6	1.0800
7	1.1896
8	1.3179
9	1.4804
10	1.5658
11	1.7236
12	1.9478
13	2.2616

According to the Fourier transform of Fig. 7.6 and the quasi-axisymmetric frequencies listed in Table 7.1, the tenth mode (Ω = 1.566) is the primary contributor to the displacements. Figure 7.7 shows the mode shape corresponding to the tenth mode. Chapter 6 showed that the response of uniform shell (h/R = 0.010) to an impulse load was dominated by modes with frequencies at Ω = 1.583 and Ω = 1.693. The shell with circumferential holes in addition to an apex hole has an impulse response frequency that has a 1.1% difference compared to the Ω = 1.583 frequency of a uniform hemispherical shell and a 7.5% difference compared to the Ω = 1.693 frequency. This shows that a uniform hemispherical shell may be used to approximate the response of a hemispherical shell with small perforations subjected to a uniform impulse load.

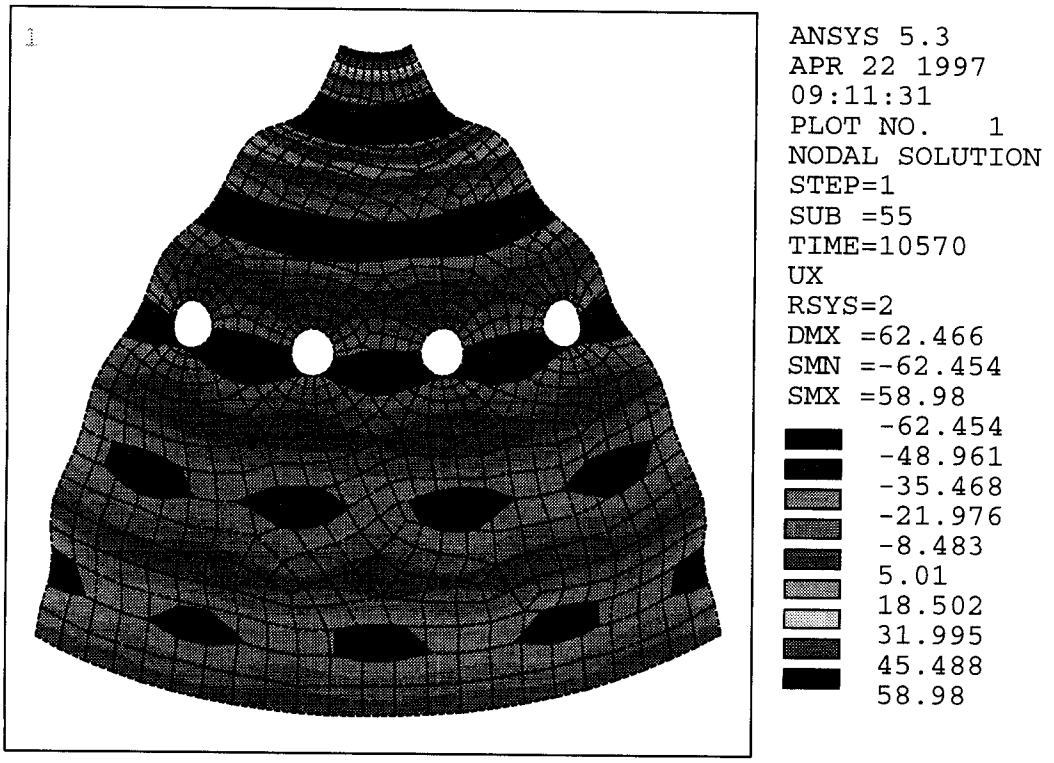

Fig. 7.7. Tenth quasi-axisymmetric mode (Ω = 1.5658). Hemispherical shell with a clamped edge and the following parameters: R = 5.0 in., h = 0.050 in., a = 0.50 in., b = 0.25 in., $E = 30.0\times10^6$ psi, $\rho = 0.733\times10^{-3}$ lb-s^2/in^4, υ = 0.3, ϕ_b = 45°.

Chapter 8

Summary and Conclusions

This research investigated the dynamic behavior of perforated clamped hemispherical shells to aid in the design of target chambers for fusion reactors. Target chambers require various perforation patterns for laser ports, diagnostic equipment, and target insertion. No work regarding the dynamic behavior of perforated hemispherical shells has been found by the author. Because of the extreme difficulty associated with deriving the general equations of motion for perforated shells, a finite element method was used in this analysis. Two specific cases of clamped perforated hemispherical shells were studied: a shell with an apex hole and a shell with twelve circumferential holes in addition to the apex hole. This research was concerned with only axisymmetric vibrations since these will be the only modes excited by a uniform radial impulse load, as seen in fusion target chamber applications. All frequencies were presented in nondimensional terms which can be applied to shells with identical geometry ratios (*a/R*, *b/R*, *h/R*).

Initially, modal analyses were performed on a clamped edge hemispherical shell with *a/R* ranging from 0.0 to 0.8, and *h/R* values of 0.005, 0.010, and 0.050. The natural frequencies of the first three axisymmetric modes were identified. Although increasing the hole radius caused an increase in the natural frequency of all modes, holes with small *a/R* values had negligible effects on frequencies. For each *h/R* value, *a/R* was taken to 0.15 with less than a 1% increase in the first three natural frequencies. Over the full range of *a/R* values tested, the thinnest shell (*h/R* = 0.005) showed the greatest increase in the frequency of the fundamental mode.

It was assumed at the beginning of this analysis that the fundamental mode would be the largest contributor to displacements resulting from a uniform radial impulsive pressure load. To verify this response, hemispherical shells with *a/R* of 0.0, 0.2, and 0.5, respectively, were subjected to a uniform radial impulse load. A *h/R* value of 0.01 was used for each shell. Since this research was concerned only with natural frequencies, damping was neglected in all transient response analyses. It was shown

that the radial displacement response over time was not uniform due to traveling wave effects. A Fourier transform was used on the response data to find approximate contributions of all modes. For all shells tested, modes higher than the fundamental were the primary contributors to radial displacement. Extended modal analyses were performed to find exact frequencies of dominant response modes. For the shell with $a/R = 0.2$ and $h/R = 0.01$, modes at $\Omega = 1.552$ and $\Omega = 1.668$ were the largest contributors to radial displacement. These frequencies were very close to the dominant response frequencies of the uniform hemispherical shell ($\Omega = 1.583$ and $\Omega = 1.693$). The response of the shell with $a/R = 0.5$ and $h/R = 0.01$ was dominated by a single mode at a significantly lower frequency of $\Omega = 1.316$.

An impulse load was also applied to a clamped hemispherical shell with twelve circumferential holes at $\phi = 45°$ in addition to the apex hole. A single clamped shell was studied with the following parameters: $a/R = 0.10$, $b/R = 0.05$, an
d $h/R = 0.1$. Because of the circumferential holes, the shell was no longer axisymmetric. However, the uniform radial impulse load did excite modes approaching an axisymmetric condition. A modal analysis was performed to identify the first 13 frequencies of these quasi-axisymmetric modes. Like the shells with an apex hole alone, a Fourier transform was used to show that modes well above the fundamental were the largest contributor to displacement. The response of the shell studied was dominated by a single quasi-axisymmetric mode at $\Omega = 1.566$.

This research has shown that the equations of motion for a uniform hemispherical shell may be used to accurately approximate the dynamic behavior of clamped perforated hemispherical shells with hole radii that are small in comparison to the shell radius, R. Although only two specific cases were studied in this analysis, the dynamic behavior of shells with similar perforation patterns may be approximated with the solution for a uniform hemispherical shell. This may be an invaluable approximation for calculating the dynamic response of the perforated shells proposed for the target chamber of the National Ignition Facility.